AIMS Mathematics, 11(8): 26640–26676.
DOI: 10.3934/math.20261069
Received: 18 May 2026
Revised: 01 August 2026
Accepted: 06 August 2026
Published: 25 August 2026

https://www.aimspress.com/journal/Math

Research article

Bifurcation and stability analysis of an SEITFR conjunctivitis model with standard incidence and treatment failure

Bashir Al-Hdaibat[1,*], Mohammad A. Safi[1], Areej Almuneef[2], Zuhur Alqahtani[2], Mahmoud H. DarAssi[3] and Omar Attoum[1]

[1] Department of Mathematics, Faculty of Science, The Hashemite University, Zarqa, Jordan

[2] Department of Mathematical Sciences, College of Science, Princess Nourah bint Abdulrahman University, P.O. Box 84428, Riyadh 11671, Saudi Arabia

[3] Department of Basic Sciences, Princess Sumaya University for Technology, Amman 11941, Jordan

* **Correspondence:** Email: b.alhdaibat@hu.edu.jo.

Abstract: This study formulates and analyzes an susceptible–exposed–infectious–treated–failed treatment–recovered (SEITFR) model for conjunctivitis transmission. The compartments represent susceptible individuals, exposed individuals, infectious cases, treated cases, detected treatment failure cases, and recovered individuals. The model separates two clinically relevant effects: Treated individuals may still transmit infection at a reduced rate, while detected treatment-failure cases are assumed to be isolated or referred for further care and therefore do not contribute directly to community transmission. We prove the positivity, boundedness, and uniqueness of solutions; derive the basic reproduction number $\mathcal{R}_0$; and establish the local stability of the disease-free equilibrium for $\mathcal{R}_0 \leq 1$ and its global stability for $\mathcal{R}_0 < 1$. The endemic equilibrium is globally asymptotically stable for $\mathcal{R}_0 > 1$ under a constant-population assumption and in the absence of immunity loss. Eigenvalue computations using the baseline loss-of-immunity rate further support the local stability of the endemic equilibrium over the tested supercritical range. A center manifold calculation for the full system confirms a forward transcritical bifurcation at $\mathcal{R}_0 = 1$. The sensitivity analysis shows that reducing contacts and residual infectiousness during treatment is essential and that increasing the treatment rate is beneficial only when treatment is accompanied by sufficient isolation or rapid clinical resolution. Numerical simulations illustrate the threshold behavior, the convergence to disease-free or endemic states, and the parameter regions where eradication is expected.

Keywords: conjunctivitis; mathematical epidemiology; treatment failure; stability analysis; forward transcritical bifurcation
Mathematics Subject Classification: 92D30, 34D20, 34C23

1. Introduction

Compartmental models provide a rigorous framework for evaluating intervention strategies in infectious disease dynamics [1]. Classical formulations often treat clinical intervention as a binary process: Infected individuals either recover or remain fully infectious [2, 3]. This simplification may miss an important intermediate stage in conjunctivitis control: Treated individuals can reduce their contacts and infectiousness but may still contribute to transmission before recovery. We address this issue by proposing a conjunctivitis model with six compartments: Susceptible (S), exposed (E), infectious (I), treated (T), failed treatment (F), and recovered (R). In the present formulation, the residual transmission reservoir is the treated class T, whereas F represents detected treatment failure cases that are isolated, referred for further management, or otherwise removed from effective community transmission. This distinction keeps the biological interpretation consistent with the standard incidence force of infection adopted in the present study.

Conjunctivitis, commonly known as "pink eye", is an inflammation of the conjunctiva characterized by redness, itching, and mucopurulent discharge [4]. Although often self-limiting, acute or poorly managed cases can result in corneal damage and permanent vision loss. The infection spreads rapidly in crowded environments, such as schools and healthcare facilities, thereby imposing significant economic and psychosocial burdens on healthcare systems [4]. Previous studies have investigated the pathophysiology of ocular inflammation, distinguishing between seasonal allergic and infectious forms of conjunctivitis [5, 6]. For viral strains, the clinical progression of acute hemorrhagic conjunctivitis (AHC) is characterized by a short incubation period of 1–3 days [7]. Furthermore, global assessments highlight a disproportionate burden of visual impairment in tropical regions, where environmental factors such as high humidity and rainfall facilitate viral persistence [8–10].

The evolution of conjunctivitis modeling has shifted from basic deterministic systems to frameworks that incorporate multiple transmission routes, nonlinear thresholds, and memory effects. Early clinical work emphasized inflammatory mechanisms [6], while deterministic SIR-type models showed how public behavior can alter epidemic estimates [11]. Threshold quantities have since become central for determining the disease's persistence and eradication [10, 12]. More recent conjunctivitis models have incorporated direct and indirect transmission [13], fractional derivatives and media awareness [14, 15], bifurcation analysis [16], and fuzzy uncertainty [17]. Related epidemic models have also examined threshold dynamics and long-term behavior in spatially diffusive and multistage settings, including degenerate diffusion [18], heterogeneous environments [19, 20], discontinuous incidence [21], and exponential convergence [22]. These studies provide useful analytical tools but they do not address the treatment failure structure considered here. Other recent works using fractional operators [23–25], residual power series methods [26], delayed interactions [27, 28], optimal control [29], and data-supported disease modeling [30] further illustrate the breadth of contemporary mathematical epidemiology.

Despite this progress, conjunctivitis models rarely distinguish between successful treatment and detected treatment failure. We therefore separate the treated class T from the failed treatment class F. The class T remains partially infectious through the factor ϵ, capturing residual shedding, imperfect adherence to hygiene recommendations, or continued close contact during treatment. The class F represents treatment failure cases that have been identified and are assumed to be isolated or referred for further clinical management; it is therefore not included in the force of infection. The model includes

constant recruitment Π, three recovery routes $(\alpha_1, \alpha_2, \alpha_3)$, treatment initiation κ, and the treatment failure rate Ψ. We derive the threshold quantity, analyze the stability under clearly stated assumptions, verify the bifurcation at $\mathcal{R}_0 = 1$, and support the analytical findings with numerical simulations.

The remainder of this paper is organized as follows. In Section 2, we present the model's formulation, providing the nonlinear differential equations and the biological justification for the T and F compartments. We also establish the mathematical well-posedness of the model by proving the positivity, boundedness, and uniqueness of solutions. In Section 3, we derive the disease-free equilibrium (DFE) and the basic reproduction number ($\mathcal{R}_0$) using the next-generation matrix method. We provide an epidemiological interpretation of $\mathcal{R}_0$ and establish the local and global stability of the DFE. We also derive the endemic equilibrium (EE). The global stability is proved only under the additional assumptions $N = N^*$ and $\delta = 0$. In Section 4, we perform a sensitivity analysis of $\mathcal{R}_0$ with respect to the model's parameters. Using the normalized sensitivity index, we quantify the relative impact of each parameter on disease transmission. These results are discussed from a public health perspective to help prioritize intervention strategies, with β identified as the primary driver of the epidemic. In Section 5, we investigate the nature of the bifurcation at the critical threshold $\mathcal{R}_0 = 1$. Using the transmission rate β as the bifurcation parameter, we compute the normal-form coefficients for the full model and show that the bifurcation is forward transcritical. In Section 6, we provide numerical simulations based on daily parameter values. The simulations illustrate the DFE threshold, the EE behavior under the assumptions used in the analysis, the numerical local stability of the EE under the baseline loss-of-immunity rate, parameter sensitivity, and the forward transcritical bifurcation. Finally, Section 7 offers concluding remarks.

2. Model formulation

We model conjunctivitis transmission by partitioning the total human population $N(t)$ into six mutually exclusive compartments: Susceptible $S(t)$, exposed $E(t)$, infectious $I(t)$, treated $T(t)$, failed treatment $F(t)$, and recovered $R(t)$. The total population is given by

$$N(t) = S(t) + E(t) + I(t) + T(t) + F(t) + R(t).$$

Susceptible individuals enter the population at a constant recruitment rate Π and experience natural mortality at rate μ, which is assumed to be the same across all compartments. Infection occurs through contact with infectious individuals according to the following force of infection:

$$\lambda(t) = \frac{\beta(I(t) + \epsilon T(t))}{N(t)}, \tag{2.1}$$

where β is the effective contact rate and $\epsilon \in (0, 1]$ is the relative infectiousness of treated individuals. Thus, $\epsilon = 1$ means that treatment does not reduce transmission, whereas smaller values describe lower infectiousness due to clinical care, hygiene, isolation, or reduced contact.

The failed treatment class F is not included in λ. In this model, F denotes detected cases for whom the first treatment did not lead directly to recovery but who are assumed to be isolated, referred for further care, or otherwise removed from effective community transmission. This assumption is consistent with public health advice that individuals with infectious conjunctivitis should reduce transmission by practicing hand hygiene, using separate towels, avoiding close contact, and remaining

at home when close contact cannot be avoided [31]. Hence, F is a clinical management class rather than an active infectious reservoir. Because this is a simplifying assumption, Section 4 also records the threshold expression for an auxiliary model in which failed treatment cases have residual infectiousness ϵ_F. This auxiliary calculation is used only as a robustness check; the main analytical results below correspond to the isolated-failure case $\epsilon_F = 0$.

Exposed individuals progress to the symptomatic infectious stage at the rate Φ. Infectious individuals either recover naturally at the rate α_1 or enter the treatment class at the rate κ. Individuals in the treatment compartment recover at the rate α_2 or move to the failed treatment class at the rate Ψ. Individuals in F eventually recover at the rate α_3. Recovered individuals lose temporary immunity at the rate δ, returning to the susceptible pool.

The dynamics of the model are described by the following system of ordinary differential equations:

$$\begin{cases} \dfrac{dS}{dt} = \Pi - (\lambda + \mu)S + \delta R, \\ \dfrac{dE}{dt} = \lambda S - (\Phi + \mu)E, \\ \dfrac{dI}{dt} = \Phi E - (\alpha_1 + \kappa + \mu)I, \\ \dfrac{dT}{dt} = \kappa I - (\alpha_2 + \Psi + \mu)T, \\ \dfrac{dF}{dt} = \Psi T - (\alpha_3 + \mu)F, \\ \dfrac{dR}{dt} = \alpha_1 I + \alpha_2 T + \alpha_3 F - (\mu + \delta)R. \end{cases} \tag{2.2}$$

The flow of individuals between compartments is illustrated in Figure 1. The model parameters are summarized in Table 1.

Table 1. Description of model parameters.

Parameters	Description
Π	Recruitment rate of susceptible individuals
μ	Natural death rate
β	Effective contact rate
ϵ	Modification factor for infectiousness of treated class
Φ	Progression rate from exposed to infectious
κ	Treatment rate for infectious individuals
Ψ	Rate of treatment failure
α_1	Natural recovery rate from I
α_2	Recovery rate from T
α_3	Recovery rate from F
δ	Rate of loss of immunity

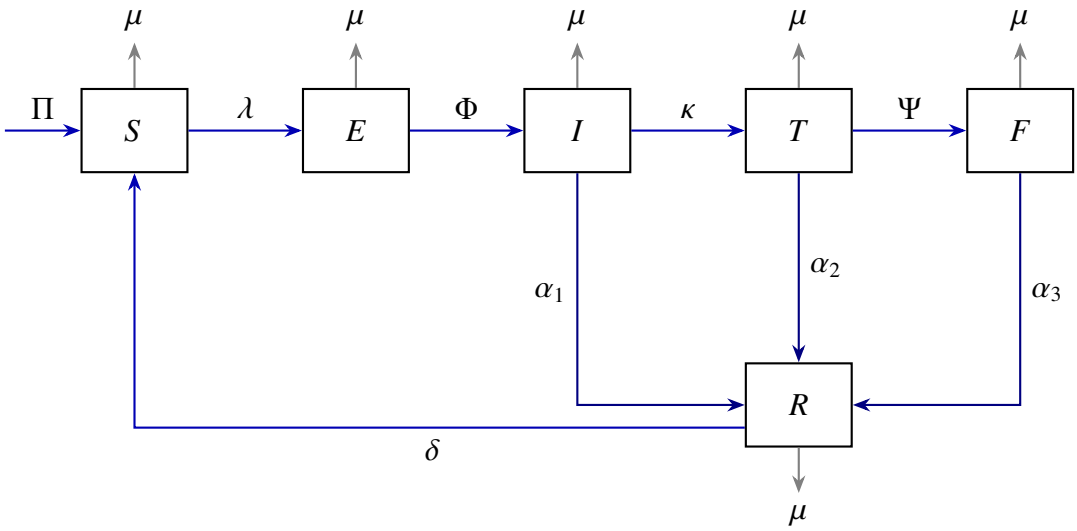

Figure 1. Flow diagram of the SEITFR model (2.2). Susceptible individuals are infected at the rate $\lambda = \beta(I + \epsilon T)/N$, where I denotes fully infectious individuals and T denotes treated individuals with reduced residual infectiousness. The failed treatment class F is assumed to be noninfectious in the main model and contributes to recovery at the rate α_3. The definitions of the state variables and parameters are given in Table 1.

2.1. Positivity of solutions

Theorem 1. *Let the initial conditions satisfy*

$$S(0) > 0, \quad E(0) \geq 0, \quad I(0) \geq 0, \quad T(0) \geq 0, \quad F(0) \geq 0, \quad R(0) \geq 0.$$

Then the solution $(S(t), E(t), I(t), T(t), F(t), R(t))^T$ *remains in the non-negative orthant* $\mathbb{R}^6_+$ *for all* $t \geq 0$.

Proof. System (2.2) can be written in the following compact form:

$$\frac{dX}{dt} = f(X), \tag{2.3}$$

where $X(t) = (S(t), E(t), I(t), T(t), F(t), R(t))^T$ and $X(0) \in \mathbb{R}^6_+$. The vector-valued function $f(X)$ is defined by

$$f(X) = \begin{pmatrix} f_1(X) \\ f_2(X) \\ f_3(X) \\ f_4(X) \\ f_5(X) \\ f_6(X) \end{pmatrix} = \begin{pmatrix} \Pi - (\lambda + \mu)S + \delta R \\ \lambda S - (\Phi + \mu)E \\ \Phi E - (\alpha_1 + \kappa + \mu)I \\ \kappa I - (\alpha_2 + \Psi + \mu)T \\ \Psi T - (\alpha_3 + \mu)F \\ \alpha_1 I + \alpha_2 T + \alpha_3 F - (\mu + \delta)R \end{pmatrix}.$$

According to the theory of ordinary differential equations, System (2.3) has a non-negative solution if and only if, for each component i, $f_i(X) \geq 0$ whenever $X_i = 0$ and $X_j \geq 0$ for all $j \neq i$ [32]. From

System (2.2), we deduce the following:

$$\begin{aligned}
\left.\frac{dS}{dt}\right|_{S=0} &= \Pi + \delta R \geq \Pi > 0,\\
\left.\frac{dE}{dt}\right|_{E=0} &= \lambda S \geq 0,\\
\left.\frac{dI}{dt}\right|_{I=0} &= \Phi E \geq 0,\\
\left.\frac{dT}{dt}\right|_{T=0} &= \kappa I \geq 0,\\
\left.\frac{dF}{dt}\right|_{F=0} &= \Psi T \geq 0,\\
\left.\frac{dR}{dt}\right|_{R=0} &= \alpha_1 I + \alpha_2 T + \alpha_3 F \geq 0.
\end{aligned}$$

Since each derivative is non-negative on the boundary of the non-negative orthant $\mathbb{R}^6_+$, the solution cannot cross into the negative region. Therefore, the non-negative orthant $\mathbb{R}^6_+$ is positively invariant, and any solution starting from non-negative initial conditions remains non-negative for all $t \geq 0$. □

2.2. Invariant region

Theorem 2. *All solutions of System* (2.2) *with non-negative initial conditions satisfy*

$$0 < \gamma \leq N(t) \leq \mathcal{M} \quad \textit{for all } t \geq 0,$$

where $\gamma = \min\left\{N(0), \frac{\Pi}{\mu}\right\}$ *and* $\mathcal{M} = \max\left\{N(0), \frac{\Pi}{\mu}\right\}$. *Consequently, the closed set*

$$\Omega = \left\{(S, E, I, T, F, R) \in \mathbb{R}^6_+ : 0 < \gamma \leq N \leq \mathcal{M}\right\}$$

is positively invariant and globally attracting.

Proof. Summing all equations in System (2.2), the rate of change of the total population $N(t)$ is given by

$$\frac{dN}{dt} = \Pi - \mu N. \tag{2.4}$$

The solution to this first-order linear differential equation is

$$N(t) = \frac{\Pi}{\mu} + \left(N(0) - \frac{\Pi}{\mu}\right)e^{-\mu t}. \tag{2.5}$$

If $N(0) > \Pi/\mu$, then $N(t)$ decreases monotonically toward the carrying capacity Π/μ as $t \to \infty$. In this case, $N(t) \leq N(0)$ for all $t \geq 0$. Conversely, if $N(0) \leq \Pi/\mu$, then $N(t)$ increases monotonically toward Π/μ, implying $N(t) \leq \Pi/\mu$ for all $t \geq 0$. Thus, for all $t \geq 0$, we have

$$N(t) \leq \max\left\{N(0), \frac{\Pi}{\mu}\right\} \equiv \mathcal{M}. \tag{2.6}$$

Furthermore, since $N(0) > 0$ and $N(t)$ is continuous, it follows from Theorem 1 and Eq (2.5) that $N(t) > 0$ for all $t \geq 0$. Specifically, the population is bounded below by

$$N(t) \geq \min\left\{N(0), \frac{\Pi}{\mu}\right\} \equiv \gamma > 0.$$

This lower bound is uniform because γ depends solely on the initial population size and the model parameters.

Therefore, all solutions starting in $\mathbb{R}^6_+$ are uniformly bounded, and the set Ω is positively invariant and globally attracting. □

2.3. Uniqueness of the solution

Theorem 3. *For any initial condition $X(0) = (S(0), E(0), I(0), T(0), F(0), R(0))^\top \in \Omega$, there is a unique solution $X(t) = (S(t), E(t), I(t), T(t), F(t), R(t))^\top$ to System (2.2) for all $t \geq 0$. This solution remains bounded in Ω.*

Proof. Let $f(X)$ denote the right-hand side of the system defined in (2.3). The linear terms in $f(X)$ are continuously differentiable and thus locally Lipschitz continuous. The only nonlinearities in the system arise from the force of infection (2.1). On the invariant set Ω established in Theorem 2, the total population satisfies

$$0 < \gamma \leq N(t) \leq \mathcal{M} < \infty \quad \text{for all } t \geq 0.$$

Because the denominator of λ is bounded away from zero, λ is well-defined and smooth on Ω. We now establish bounds for the partial derivatives of λ on Ω.

Given $0 \leq I, T \leq N$ and $\epsilon \in (0, 1]$, it follows that $I + \epsilon T \leq (1 + \epsilon)N$. For any state variable $X_i \in \{S, E, F, R\}$, we have

$$\left|\frac{\partial \lambda}{\partial X_i}\right| = \left|-\frac{\beta(I + \epsilon T)}{N^2}\frac{\partial N}{\partial X_i}\right| = \frac{\beta(I + \epsilon T)}{N^2} \leq \frac{\beta(1 + \epsilon)}{N} \leq \frac{\beta(1 + \epsilon)}{\gamma} < \infty.$$

For the infectious class I, we have

$$\left|\frac{\partial \lambda}{\partial I}\right| = \left|\frac{\beta}{N} - \frac{\beta(I + \epsilon T)}{N^2}\right| \leq \frac{\beta}{N} + \frac{\beta(I + \epsilon T)}{N^2} \leq \frac{\beta(2 + \epsilon)}{N} \leq \frac{\beta(2 + \epsilon)}{\gamma} < \infty.$$

For the treated class T, we have

$$\left|\frac{\partial \lambda}{\partial T}\right| = \left|\frac{\beta\epsilon}{N} - \frac{\beta(I + \epsilon T)}{N^2}\right| \leq \frac{\beta\epsilon}{N} + \frac{\beta(I + \epsilon T)}{N^2} \leq \frac{\beta(1 + 2\epsilon)}{N} \leq \frac{\beta(1 + 2\epsilon)}{\gamma} < \infty.$$

Setting $\Gamma = \frac{\beta(2+\epsilon)}{\gamma}$, we obtain the uniform bound

$$\left|\frac{\partial \lambda}{\partial X_i}\right| \leq \Gamma < \infty \text{ for all } X_i \in \{S, E, I, T, F, R\}.$$

Since all partial derivatives of $f(X)$ are bounded on Ω, the function f is Lipschitz continuous on Ω. By the Picard–Lindelöf theorem [32], for any initial condition $X(0) \in \Omega$, there is a unique local solution $X(t)$ on the interval $[0, t_{\max})$. Furthermore, since the solutions are uniformly bounded (Theorem 2), they do not blow up in finite time, ensuring the solution exists globally for all $t \geq 0$. □

By Theorems 1–3, the mathematical and biological consistency of System (2.2) is rigorously established.

3. Equilibrium analysis and the basic reproduction number

3.1. The disease-free equilibrium (DFE)

At the DFE, the infected compartments vanish; that is, $E = I = T = F = 0$. Substituting these values into System (2.2) yields

$$0 = \Pi - \mu S^0 + \delta R^0, \qquad 0 = -(\mu + \delta)R^0.$$

This implies $R^0 = 0$ and $S^0 = \Pi/\mu$. The existence of the DFE is summarized in the following theorem.

Theorem 4. *The DFE of System* (2.2) *exists for all parameter values and is given by*

$$P_0 = \left(S^0, E^0, I^0, T^0, F^0, R^0\right) = \left(\frac{\Pi}{\mu}, 0, 0, 0, 0, 0\right). \tag{3.1}$$

In epidemiology, the basic reproduction number, $\mathcal{R}_0$, is a fundamental threshold parameter used to quantify the transmission potential of an infectious agent. It determines whether the disease will persist in the population or be eradicated.

3.2. The basic reproduction number $\mathcal{R}_0$

Theorem 5. *The basic reproduction number $\mathcal{R}_0$ for System* (2.2) *is*

$$\mathcal{R}_0 = \frac{\beta\Phi}{(\Phi + \mu)(\alpha_1 + \kappa + \mu)}\left(1 + \frac{\epsilon\kappa}{\alpha_2 + \Psi + \mu}\right). \tag{3.2}$$

Proof. To derive $\mathcal{R}_0$, we use the next-generation matrix method [33, 34]. The relevant infected compartments are E, I, and T. Note that F is excluded because it is assumed to be noninfectious. Let $\mathcal{F}$ denote the matrix of new infections and $\mathcal{V}$ the matrix of transition rates

$$\mathcal{F} = \begin{pmatrix} \lambda S \\ 0 \\ 0 \end{pmatrix}, \qquad \mathcal{V} = \begin{pmatrix} d_1 E \\ -\Phi E + d_2 I \\ -\kappa I + d_3 T \end{pmatrix},$$

where

$$d_1 = \Phi + \mu, \quad d_2 = \alpha_1 + \kappa + \mu, \quad d_3 = \alpha_2 + \Psi + \mu. \tag{3.3}$$

At the DFE, $S^0 = \Pi/\mu$ and $N^0 = \Pi/\mu$, which implies $S^0/N^0 = 1$. The Jacobian matrices F and V evaluated at P_0 are

$$F = \begin{pmatrix} 0 & \beta & \beta\epsilon \\ 0 & 0 & 0 \\ 0 & 0 & 0 \end{pmatrix}, \qquad V = \begin{pmatrix} d_1 & 0 & 0 \\ -\Phi & d_2 & 0 \\ 0 & -\kappa & d_3 \end{pmatrix}.$$

The inverse of the transition matrix V is

$$V^{-1} = \begin{pmatrix} \frac{1}{d_1} & 0 & 0 \\ \frac{\Phi}{d_1 d_2} & \frac{1}{d_2} & 0 \\ \frac{\Phi\kappa}{d_1 d_2 d_3} & \frac{\kappa}{d_2 d_3} & \frac{1}{d_3} \end{pmatrix}.$$

The next-generation matrix FV^{-1} is

$$FV^{-1} = \begin{pmatrix} \frac{\beta\Phi}{d_1 d_2}\left(1+\frac{\epsilon\kappa}{d_3}\right) & \frac{\beta}{d_2}\left(1+\frac{\epsilon\kappa}{d_3}\right) & \frac{\beta\epsilon}{d_3} \\ 0 & 0 & 0 \\ 0 & 0 & 0 \end{pmatrix}.$$

Therefore, the eigenvalues of FV^{-1} are

$$\left\{\frac{\beta\Phi}{d_1 d_2}\left(1+\frac{\epsilon\kappa}{d_3}\right),\ 0,\ 0\right\}.$$

The basic reproduction number is the spectral radius $\rho(FV^{-1})$ and is therefore equal to the nonzero eigenvalue

$$\mathcal{R}_0 := \frac{\beta\Phi}{d_1 d_2}\left(1+\frac{\epsilon\kappa}{d_3}\right) = \frac{\beta\Phi}{(\Phi+\mu)(\alpha_1+\kappa+\mu)}\left(1+\frac{\epsilon\kappa}{\alpha_2+\Psi+\mu}\right).$$

□

The basic reproduction number $\mathcal{R}_0$ admits a clear epidemiological interpretation. The first term

$$\mathcal{R}_0^{(I)} = \frac{\beta\Phi}{(\Phi+\mu)(\alpha_1+\kappa+\mu)},$$

represents the contribution of the infectious class I: An exposed individual survives the latency period with probability $\Phi/(\Phi+\mu)$ and, during their infectious period $(1/(\alpha_1+\kappa+\mu))$, transmits the infection at rate β. The second term,

$$\mathcal{R}_0^{(T)} = \mathcal{R}_0^{(I)} \cdot \frac{\epsilon\kappa}{\alpha_2+\Psi+\mu},$$

accounts for the contribution of treated individuals. Following the infectious stage, an individual enters treatment with probability $\kappa/(\alpha_1+\kappa+\mu)$. Once in the treatment class, they transmit at a modified rate $\epsilon\beta$ for an average duration of $1/(\alpha_2+\Psi+\mu)$. Consequently, the total transmission potential is the sum $\mathcal{R}_0 = \mathcal{R}_0^{(I)} + \mathcal{R}_0^{(T)}$.

The exclusion of F from the next-generation matrix follows from the modeling assumption that failed treatment cases are detected and removed from effective community transmission. If failed treatment individuals were assumed to retain residual infectiousness, the force of infection could be written as

$$\lambda_F = \frac{\beta(I+\epsilon T+\epsilon_F F)}{N}, \tag{3.4}$$

where $\epsilon_F \geq 0$ is the relative infectiousness of F. In that auxiliary model, the reproduction number becomes

$$\mathcal{R}_0^F = \frac{\beta\Phi}{(\Phi+\mu)(\alpha_1+\kappa+\mu)}\left(1+\frac{\epsilon\kappa}{\alpha_2+\Psi+\mu}+\frac{\epsilon_F\Psi\kappa}{(\alpha_2+\Psi+\mu)(\alpha_3+\mu)}\right). \tag{3.5}$$

Thus, the main model corresponds to the special case $\epsilon_F = 0$. Any positive value of ϵ_F increases the reproduction number and lowers the admissible eradication threshold for β. This expression is used again in the sensitivity discussion as a robustness check, while the main stability and bifurcation results are proved for the isolated failure setting.

3.3. Stability analysis of the DFE

Theorem 6. *The DFE P_0 is locally asymptotically stable if $\mathcal{R}_0 < 1$ and unstable if $\mathcal{R}_0 > 1$.*

Proof. The Jacobian matrix of System (2.2), evaluated at the DFE P_0, is

$$J(P_0) = \begin{pmatrix} -\mu & 0 & -\beta & -\beta\epsilon & 0 & \delta \\ 0 & -(\Phi+\mu) & \beta & \beta\epsilon & 0 & 0 \\ 0 & \Phi & -(\alpha_1+\kappa+\mu) & 0 & 0 & 0 \\ 0 & 0 & \kappa & -(\alpha_2+\Psi+\mu) & 0 & 0 \\ 0 & 0 & 0 & \Psi & -(\alpha_3+\mu) & 0 \\ 0 & 0 & \alpha_1 & \alpha_2 & \alpha_3 & -(\mu+\delta) \end{pmatrix}. \tag{3.6}$$

The block-triangular structure of $J(P_0)$ yields the following three immediate negative eigenvalues:

$$\sigma_1 = -\mu, \quad \sigma_2 = -(\mu+\delta), \quad \sigma_3 = -(\alpha_3+\mu).$$

The remaining eigenvalues are determined by the submatrix J_x corresponding to the infected classes $x = (E, I, T)^{\mathrm{T}}$

$$J_x = \begin{pmatrix} -d_1 & \beta & \beta\epsilon \\ \Phi & -d_2 & 0 \\ 0 & \kappa & -d_3 \end{pmatrix},$$

where d_1, d_2, and d_3 are given in (3.3). The characteristic polynomial of J_x is given by

$$P(\sigma) = \sigma^3 + a_1\sigma^2 + a_2\sigma + a_3,$$

with the coefficients

$$\begin{aligned} a_1 &= d_1 + d_2 + d_3, \\ a_2 &= d_1d_2 + d_1d_3 + d_2d_3 - \beta\Phi, \\ a_3 &= d_1d_2d_3 - \beta\Phi d_3 - \beta\epsilon\Phi\kappa = d_1d_2d_3(1-\mathcal{R}_0), \end{aligned}$$

where

$$\mathcal{R}_0 = \frac{\beta\Phi}{d_1d_2} + \frac{\beta\epsilon\Phi\kappa}{d_1d_2d_3}. \tag{3.7}$$

By the Routh–Hurwitz criterion [35], all eigenvalues have negative real parts if $a_1 > 0$, $a_3 > 0$, and $a_1a_2 > a_3$. Given that all parameters are positive, $a_1 > 0$ is trivially satisfied. The condition $a_3 > 0$ holds if and only if $\mathcal{R}_0 < 1$. To verify the third condition, we evaluate the difference $a_1a_2 - a_3$

$$\begin{aligned} a_1a_2 - a_3 &= (d_1+d_2+d_3)(d_1d_2 + d_1d_3 + d_2d_3 - \beta\Phi) - (d_1d_2d_3 - \beta\Phi d_3 - \beta\epsilon\Phi\kappa) \\ &= (d_1+d_2)(d_1d_2 - \beta\Phi) + d_1^2d_3 + d_2^2d_3 + d_1d_3^2 + d_2d_3^2 + 2d_1d_2d_3 + \beta\epsilon\Phi\kappa. \end{aligned}$$

When $\mathcal{R}_0 < 1$, the definition of $\mathcal{R}_0$ in Eq (3.7) implies

$$0 < \frac{\beta\Phi}{d_1d_2} < \mathcal{R}_0 < 1.$$

This ensures that $d_1d_2 - \beta\Phi > 0$. Since all parameters and remaining terms are positive, it follows that $a_1a_2 - a_3 > 0$ whenever $\mathcal{R}_0 < 1$. Conversely, if $\mathcal{R}_0 > 1$, then $a_3 < 0$, ensuring at least one eigenvalue with a positive real part. Thus, P_0 is locally asymptotically stable if $\mathcal{R}_0 < 1$ and unstable if $\mathcal{R}_0 > 1$. □

At the critical threshold $\mathcal{R}_0 = 1$, the DFE is nonhyperbolic and is therefore not covered by Theorem 6. We apply the boundary-equilibrium criterion in [36] to complete the local stability analysis at $\mathcal{R}_0 = 1$. The critical transmission rate for which $\mathcal{R}_0 = 1$ is

$$\beta_c = \frac{d_1 d_2 d_3}{\Phi(d_3 + \epsilon\kappa)}, \tag{3.8}$$

where d_1, d_2, and d_3 are defined in (3.3).

Theorem 7. *If $\mathcal{R}_0 = 1$, then the DFE P_0 is locally asymptotically stable in the feasible region Ω.*

Proof. To apply Theorem 2 of [36], partition the state variables as follows:

$$x = (E, I, T)^\top, \qquad y = (S, F, R)^\top, \qquad y^0 = \left(\frac{\Pi}{\mu}, 0, 0\right)^\top.$$

In these coordinates, System (2.2) has the form

$$\dot{x} = f(x, y), \qquad \dot{y} = g(x, y),$$

and the DFE given in Theorem 4 has the boundary-equilibrium form

$$(x, y) = (0, y^0).$$

We first verify Assumptions (B1)–(B6) of [36]. By Theorem 4,

$$f(0, y^0) = 0, \qquad g(0, y^0) = 0.$$

Moreover, since $N^0 = \Pi/\mu > 0$, there is a neighborhood U of P_0 in which N is bounded away from zero. Hence, the right-hand side of System (2.2) is of class C^2 on U. In addition, the feasible region Ω is positively invariant by Theorems 1 and 2. Since Theorem 2 of [36] is a local result, it can be applied on $U \cap \Omega$. Thus, the local regularity and invariance requirements in (B1) and (B2) are satisfied.

The matrix

$$A = D_x f(0, y^0)$$

is the infected block J_x obtained in the proof of Theorem 6, evaluated at $\beta = \beta_c$. Its off-diagonal entries are non-negative, and the transitions

$$E \longrightarrow I, \qquad I \longrightarrow E, \qquad I \longrightarrow T, \qquad T \longrightarrow E$$

make its associated directed graph strongly connected. Thus, A is cooperative and irreducible, which verifies (B3).

The regular splitting of A, together with the non-negativity of the new-infection matrix and the inverse of the transition matrix, was established in the proof of Theorem 5. The spectral radius of the corresponding next-generation matrix is $\mathcal{R}_0$ given in (3.2). Therefore, (B4) also holds.

The remaining Jacobian blocks at the DFE are

$$\begin{aligned}
\mathsf{B} &= D_y f(0, y^0) = 0_{3\times 3},\\
\mathsf{C} &= D_x g(0, y^0) = \begin{pmatrix} 0 & -\beta_c & -\beta_c\epsilon \\ 0 & 0 & \Psi \\ 0 & \alpha_1 & \alpha_2 \end{pmatrix},\\
\mathsf{D} &= D_y g(0, y^0) = \begin{pmatrix} -\mu & 0 & \delta \\ 0 & -(\alpha_3+\mu) & 0 \\ 0 & \alpha_3 & -(\mu+\delta) \end{pmatrix}.
\end{aligned} \tag{3.9}$$

In particular, we have

$$\det(\mathsf{D}) = -\mu(\alpha_3+\mu)(\mu+\delta) \neq 0.$$

Hence, $\mathsf{B} = 0$ and D is invertible, verifying (B5) and (B6).

At $\mathcal{R}_0 = 1$, Theorem 2 of [36] ensures that zero is a simple eigenvalue of A. Using (3.3) and (3.2), positive right and left zero eigenvectors may be chosen as

$$q_x = \begin{pmatrix} \dfrac{d_2}{\Phi} \\ 1 \\ \dfrac{\kappa}{d_3} \end{pmatrix} = \begin{pmatrix} q_E \\ q_I \\ q_T \end{pmatrix}, \qquad p_x = \omega \begin{pmatrix} 1 \\ \dfrac{d_1}{\Phi} \\ \dfrac{\beta_c\epsilon}{d_3} \end{pmatrix}, \tag{3.10}$$

where

$$\omega = \left(\frac{d_1+d_2}{\Phi} + \frac{\beta_c\epsilon\kappa}{d_3^2} \right)^{-1} > 0. \tag{3.11}$$

Thus

$$Aq_x = 0, \qquad p_x^\top A = 0, \qquad p_x^\top q_x = 1.$$

Let

$$\eta = -\mathsf{D}^{-1}\mathsf{C}q_x = (\eta_S, \eta_F, \eta_R)^\top$$

be the correction associated with the variables in y. From (3.9) and (3.10), we obtain

$$\eta_F = \frac{\Psi\kappa}{d_3(\alpha_3+\mu)}, \qquad \eta_R = \frac{\alpha_1 + \dfrac{\alpha_2\kappa}{d_3} + \dfrac{\alpha_3\Psi\kappa}{d_3(\alpha_3+\mu)}}{\mu+\delta}. \tag{3.12}$$

In the original ordering (S, E, I, T, F, R), the corresponding full right zero eigenvector is

$$\widehat{q} = (\eta_S, q_E, q_I, q_T, \eta_F, \eta_R)^\top.$$

Since the total population satisfies (2.4), the Jacobian at the critical point satisfies

$$\mathbf{1}^\top J(P_0, \beta_c) = -\mu\mathbf{1}^\top, \qquad \mathbf{1} = (1,1,1,1,1,1)^\top.$$

Using

$$J(P_0, \beta_c)\widehat{q} = 0,$$

we obtain

$$0 = \mathbf{1}^\top J(P_0, \beta_c)\widehat{q} = -\mu \mathbf{1}^\top \widehat{q}.$$

Therefore, we have

$$\eta_S + q_E + q_I + q_T + \eta_F + \eta_R = 0,$$

and hence

$$\eta_S = -(q_E + q_I + q_T + \eta_F + \eta_R) < 0. \tag{3.13}$$

Following Theorem 2 of [36], denote the threshold coefficient as

$$\begin{aligned} \ell := \sum_{i=1}^{3} (p_x)_i \Bigg[& \sum_{j,k=1}^{3} \frac{\partial^2 f_i}{\partial x_j \partial x_k}(0, y^0)(q_x)_j (q_x)_k \\ & + 2 \sum_{j=1}^{3} \sum_{r=1}^{3} \frac{\partial^2 f_i}{\partial x_j \partial y_r}(0, y^0)(q_x)_j \eta_r \\ & + \sum_{r,s=1}^{3} \frac{\partial^2 f_i}{\partial y_r \partial y_s}(0, y^0)\eta_r \eta_s \Bigg]. \end{aligned} \tag{3.14}$$

Only the Exposed equation contains nonlinear terms. Using (2.1), (3.10), and (3.13), Eq (3.14) reduces to

$$\begin{aligned} \ell &= \frac{2\beta_c \omega}{N^0}(q_I + \epsilon q_T)\eta_S \\ &= \frac{2\beta_c \omega}{N^0}\left(1 + \frac{\epsilon\kappa}{d_3}\right)\eta_S. \end{aligned} \tag{3.15}$$

All factors in (3.15), except η_S, are positive, whereas $\eta_S < 0$ by (3.13). Therefore, we have

$$\ell < 0.$$

The conclusion now follows directly from Theorem 2 of [36]. □

Theorem 8. *If $\mathcal{R}_0 < 1$, the DFE P_0 is globally asymptotically stable in the feasible region Ω.*

Proof. Define

$$L = E + \frac{d_1}{\Phi} I + \frac{\beta\epsilon}{d_3} T,$$

where d_1, d_2, and d_3 are defined in (3.3). The function L is non-negative in Ω and vanishes only when $E = I = T = 0$. Along with the solutions of (2.2), we have

$$\begin{aligned} \dot{L} &= \lambda S - d_1 E + \frac{d_1}{\Phi}(\Phi E - d_2 I) + \frac{\beta\epsilon}{d_3}(\kappa I - d_3 T) \\ &= \frac{\beta S}{N}(I + \epsilon T) - \frac{d_1 d_2}{\Phi} I + \frac{\beta\epsilon\kappa}{d_3} I - \beta\epsilon T, \\ &= \left(\frac{S}{N}\beta + \frac{\beta\epsilon\kappa}{d_3} - \frac{d_1 d_2}{\Phi}\right) I + \beta\epsilon\left(\frac{S}{N} - 1\right) T. \end{aligned} \tag{3.16}$$

Since $0 \leq S/N \leq 1$ in Ω and using (3.7), it follows that

$$\dot{L} \leq \left(\beta + \frac{\beta\epsilon\kappa}{d_3} - \frac{d_1 d_2}{\Phi}\right) I = \frac{d_1 d_2}{\Phi}(\mathcal{R}_0 - 1)I. \tag{3.17}$$

Thus $\dot{L} \leq 0$ whenever $\mathcal{R}_0 < 1$.

It remains to identify the largest invariant set contained in $\{\dot{L} = 0\}$. If $\mathcal{R}_0 < 1$, Inequality (3.17) implies that $I = 0$ on this set. On any invariant subset of $\{\dot{L} = 0\}$, the equation for I in System (2.2) then gives $\Phi E = 0$; hence $E = 0$. Moreover, the exact expression (3.16) implies that $T = 0$. Therefore, the largest invariant set contained in $\{\dot{L} = 0\}$ is $\mathcal{M} = \{(S, E, I, T, F, R) \in \Omega : E = I = T = 0\}$. On $\mathcal{M}$, the equation for F becomes $\dot{F} = -(\alpha_3 + \mu)F$, and hence $F(t) \to 0$ as $t \to \infty$. The equation for R then implies that $R(t) \to 0$. Finally, the susceptible equation reduces asymptotically to $\dot{S} = \Pi - \mu S$, so that $S(t) \to \Pi/\mu$.

By LaSalle's invariance principle [37], every solution in Ω approaches $\mathcal{M}$. Since every trajectory in $\mathcal{M}$ converges to P_0, it follows that every solution in Ω approaches P_0 as $t \to \infty$. Therefore, the DFE is globally asymptotically stable in Ω whenever $\mathcal{R}_0 < 1$. □

3.4. Endemic equilibrium (EE)

Theorem 9. *If $\mathcal{R}_0 > 1$, System* (2.2) *admits a unique positive EE $P^* = (S^*, E^*, I^*, T^*, F^*, R^*)$, where*

$$\begin{aligned}
S^* &= \frac{\Pi}{\mu\mathcal{R}_0}, \\
I^* &= \frac{\Pi(\mathcal{R}_0 - 1)}{\mu\mathcal{R}_0(\Theta_I + \Theta_R)}, \\
E^* &= \frac{\alpha_1 + \kappa + \mu}{\Phi} I^*, \\
T^* &= \frac{\kappa}{\alpha_2 + \Psi + \mu} I^*, \\
F^* &= \frac{\Psi\kappa}{(\alpha_2 + \Psi + \mu)(\alpha_3 + \mu)} I^*, \\
R^* &= \Theta_R I^*,
\end{aligned} \tag{3.18}$$

where the auxiliary constants are defined by

$$\Theta_I = \frac{\alpha_1 + \kappa + \mu}{\Phi} + 1 + \frac{\kappa}{\alpha_2 + \Psi + \mu} + \frac{\Psi\kappa}{(\alpha_2 + \Psi + \mu)(\alpha_3 + \mu)}, \tag{3.19}$$

$$\Theta_R = \frac{1}{\mu + \delta}\left[\alpha_1 + \frac{\alpha_2\kappa}{\alpha_2 + \Psi + \mu} + \frac{\alpha_3\Psi\kappa}{(\alpha_2 + \Psi + \mu)(\alpha_3 + \mu)}\right]. \tag{3.20}$$

Proof. At the EE, the state variables are constant; hence, all time derivatives in System (2.2) vanish. This leads to the following set of equilibrium equations:

$$\Pi = (\lambda^* + \mu)S^* - \delta R^*, \tag{3.21}$$

$$\lambda^* S^* = (\Phi + \mu)E^*, \tag{3.22}$$

$$\Phi E^* = (\alpha_1 + \kappa + \mu)I^*, \tag{3.23}$$

$$\kappa I^* = (\alpha_2 + \Psi + \mu)T^*, \tag{3.24}$$

$$\Psi T^* = (\alpha_3 + \mu)F^*, \tag{3.25}$$

$$\alpha_1 I^* + \alpha_2 T^* + \alpha_3 F^* = (\mu + \delta)R^*, \tag{3.26}$$

where the force of infection λ^* and the total population N^* at equilibrium are defined in (3.27) and (3.28), respectively, as follows:

$$\lambda^* = \frac{\beta(I^* + \epsilon T^*)}{N^*}, \tag{3.27}$$

$$N^* = S^* + E^* + I^* + T^* + F^* + R^*. \tag{3.28}$$

Summing all equations in System (2.2) at equilibrium yields $0 = \Pi - \mu N^*$, which implies

$$N^* = \frac{\Pi}{\mu}. \tag{3.29}$$

From Eqs (3.23)–(3.25), we express E^*, T^*, and F^* in terms of I^*

$$E^* = \frac{\alpha_1 + \kappa + \mu}{\Phi} I^*, \quad T^* = \frac{\kappa}{\alpha_2 + \Psi + \mu} I^*, \quad F^* = \frac{\Psi\kappa}{(\alpha_2 + \Psi + \mu)(\alpha_3 + \mu)} I^*. \tag{3.30}$$

Substituting these into Eq (3.26) leads directly to the following expression for R^*

$$R^* = \frac{1}{\mu + \delta}\left[\alpha_1 + \frac{\alpha_2\kappa}{\alpha_2 + \Psi + \mu} + \frac{\alpha_3\Psi\kappa}{(\alpha_2 + \Psi + \mu)(\alpha_3 + \mu)}\right] I^* = \Theta_R I^*. \tag{3.31}$$

Using the definition of λ^* in (3.27) together with the expression for T^* from (3.30), the force of infection can be written as

$$\lambda^* = \frac{\beta I^*}{N^*}\left(1 + \frac{\epsilon\kappa}{\alpha_2 + \Psi + \mu}\right). \tag{3.32}$$

Equating the expression for $\lambda^* S^*$ from (3.22) with the expression for E^* in (3.30) gives

$$\left[\frac{\beta I^*}{N^*}\left(1 + \frac{\epsilon\kappa}{\alpha_2 + \Psi + \mu}\right)\right] S^* = \frac{(\Phi + \mu)(\alpha_1 + \kappa + \mu)}{\Phi} I^*. \tag{3.33}$$

Canceling $I^* > 0$ and solving for S^* confirms the relationship with the reproduction number

$$S^* = \frac{N^*}{\left[\frac{\beta\Phi\left(1 + \frac{\epsilon\kappa}{\alpha_2 + \Psi + \mu}\right)}{(\Phi + \mu)(\alpha_1 + \kappa + \mu)}\right]} = \frac{N^*}{\mathcal{R}_0}. \tag{3.34}$$

We now substitute all expressed compartments into the conservation equation for N^* in (3.28)

$$N^* = S^* + (E^* + I^* + T^* + F^*) + R^* = \frac{N^*}{\mathcal{R}_0} + \Theta_I I^* + \Theta_R I^*, \tag{3.35}$$

where Θ_I is the sum of the coefficients for (E^*, I^*, T^*, F^*) derived in (3.30). Rearranging gives

$$N^*\left(1 - \frac{1}{\mathcal{R}_0}\right) = (\Theta_I + \Theta_R)I^* \implies N^* = \frac{(\Theta_I + \Theta_R)\mathcal{R}_0}{\mathcal{R}_0 - 1} I^*. \tag{3.36}$$

Combining the total population size from (3.29) with (3.36) gives the following equilibrium value for I^*

$$I^* = \frac{\Pi(\mathcal{R}_0 - 1)}{\mu\mathcal{R}_0(\Theta_I + \Theta_R)}. \tag{3.37}$$

Since $\mathcal{R}_0 > 1$, it follows that $I^* > 0$. All other state variables are positive linear multiples of I^*, thereby ensuring the existence of a unique positive EE P^*. □

3.5. Stability of the EE

For the present conjunctivitis model (2.2), proving the global stability of the EE is nontrivial because the standard incidence force of infection depends on both the fully infectious class I and the treated class T with reduced infectiousness. To facilitate the Lyapunov analysis, we first establish a structural identity that expresses the ratio λ/λ^* as a weighted average of the normalized infectious components I/I^* and T/T^*. This identity allows the transmission terms to be handled in a balanced form and is essential for applying the arithmetic mean–geometric mean (AM–GM) inequality in the global stability proof.

Lemma 1. *Assume that the total population remains at its equilibrium value, $N = N^*$. Then $\frac{\lambda}{\lambda^*}$ satisfies the convex identity*

$$\frac{\lambda}{\lambda^*} = W_I\left(\frac{I}{I^*}\right) + W_T\left(\frac{T}{T^*}\right), \tag{3.38}$$

where the weights $W_I, W_T \in (0,1)$ represent the relative contribution of each infectious class to total transmission at the EE P^*:

$$W_I = \frac{\beta I^*}{\lambda^* N^*}, \quad W_T = \frac{\beta\epsilon T^*}{\lambda^* N^*}, \quad \textit{and} \quad W_I + W_T = 1. \tag{3.39}$$

Proof. Consider the force of infection at an arbitrary state and at equilibrium as follows:

$$\lambda = \frac{\beta(I + \epsilon T)}{N} \quad \text{and} \quad \lambda^* = \frac{\beta(I^* + \epsilon T^*)}{N^*}.$$

From the equilibrium relation for λ^*, it follows that

$$\lambda^* N^* = \beta I^* + \beta\epsilon T^*. \tag{3.40}$$

Dividing both sides of (3.40) by $\lambda^* N^*$ confirms that the weights sum to one

$$1 = \frac{\beta I^* + \beta\epsilon T^*}{\lambda^* N^*} = \frac{\beta I^*}{\lambda^* N^*} + \frac{\beta\epsilon T^*}{\lambda^* N^*} = W_I + W_T.$$

Finally, normalizing λ with respect to λ^* and assuming $N = N^*$, we use (3.40) to obtain

$$\begin{aligned}
\frac{\lambda}{\lambda^*} &= \frac{\beta(I + \epsilon T)}{\beta(I^* + \epsilon T^*)} \\
&= \frac{\beta(I + \epsilon T)}{\lambda^* N^*} \\
&= \frac{\beta I}{\lambda^* N^*} + \frac{\beta\epsilon T}{\lambda^* N^*} \\
&= \left(\frac{\beta I^*}{\lambda^* N^*}\right)\frac{I}{I^*} + \left(\frac{\beta\epsilon T^*}{\lambda^* N^*}\right)\frac{T}{T^*} \\
&= W_I\left(\frac{I}{I^*}\right) + W_T\left(\frac{T}{T^*}\right).
\end{aligned}$$

□

Theorem 10. *Assume that $\mathcal{R}_0 > 1$, $\delta = 0$, and $N(0) = N^* = \Pi/\mu$. Then the unique EE P^* is globally asymptotically stable in the positive interior of the reduced feasible region*

$$\Omega^* = \{(S, E, I, T, F, R) \in \mathbb{R}^6_+ : N = N^*\}.$$

Equivalently, every solution in this reduced region with $S(0), E(0), I(0), T(0) > 0$ converges to P^*.

Proof. Define the Volterra-type Lyapunov function $L = L_S + L_E + L_I + L_T$, where

$$L = S^* G\left(\frac{S}{S^*}\right) + E^* G\left(\frac{E}{E^*}\right) + \frac{\lambda^* S^*}{\Phi E^*} I^* G\left(\frac{I}{I^*}\right) + \frac{W_T \lambda^* S^*}{\kappa I^*} T^* G\left(\frac{T}{T^*}\right), \tag{3.41}$$

and $G(x) = x - 1 - \ln x$.

The coefficients are chosen in accordance with the equilibrium conditions as follows:

$$\Pi = \lambda^* S^* + \mu S^* \tag{3.42}$$

$$\lambda^* S^* = (\Phi + \mu) E^* \Longrightarrow \Phi + \mu = \frac{\lambda^* S^*}{E^*} \tag{3.43}$$

$$\Phi E^* = (\alpha_1 + \kappa + \mu) I^* \Rightarrow \alpha_1 + \kappa + \mu = \frac{\Phi E^*}{I^*} \tag{3.44}$$

$$\kappa I^* = (\alpha_2 + \Psi + \mu) T^* \Rightarrow \alpha_2 + \Psi + \mu = \frac{\kappa I^*}{T^*}. \tag{3.45}$$

We compute the time derivative of each component of L along solutions of System (2.2).

Using $\dot{S} = \Pi - \lambda S - \mu S$ and the equilibrium relation (3.42), we have

$$\begin{aligned}
\dot{L}_S &= \left(1 - \frac{S^*}{S}\right) \dot{S} \\
&= \left(1 - \frac{S^*}{S}\right) (\lambda^* S^* + \mu S^* - \lambda S - \mu S) \\
&= \left(1 - \frac{S^*}{S}\right) \left[-\mu (S - S^*) + \lambda^* S^* \left(1 - \frac{\lambda S}{\lambda^* S^*}\right)\right] \\
&= -\mu \frac{(S - S^*)^2}{S} + \lambda^* S^* \left(1 - \frac{S^*}{S} - \frac{\lambda S}{\lambda^* S^*} + \frac{\lambda}{\lambda^*}\right).
\end{aligned} \tag{3.46}$$

Using $\dot{E} = \lambda S - (\Phi + \mu) E$ and the equilibrium relation (3.43), we have

$$\begin{aligned}
\dot{L}_E &= \left(1 - \frac{E^*}{E}\right) \dot{E} \\
&= \left(1 - \frac{E^*}{E}\right) \left(\lambda S - \frac{\lambda^* S^*}{E^*} E\right) \\
&= \left(1 - \frac{E^*}{E}\right) \left[\lambda^* S^* \left(\frac{\lambda S}{\lambda^* S^*} - \frac{E}{E^*}\right)\right] \\
&= \lambda^* S^* \left(1 - \frac{E}{E^*} - \frac{\lambda S E^*}{\lambda^* S^* E} + \frac{\lambda S}{\lambda^* S^*}\right).
\end{aligned} \tag{3.47}$$

Using $\dot{I} = \Phi E - (\alpha_1 + \kappa + \mu)I$ and the equilibrium relation (3.44), we have

$$\begin{aligned}
\dot{L}_I &= \frac{\lambda^* S^*}{\Phi E^*}\left(1 - \frac{I^*}{I}\right)\dot{I} \\
&= \frac{\lambda^* S^*}{\Phi E^*}\left(1 - \frac{I^*}{I}\right)\left(\Phi E - \frac{\Phi E^*}{I^*} I\right) \\
&= \frac{\lambda^* S^*}{\Phi E^*}\left(1 - \frac{I^*}{I}\right)\left[\Phi E^*\left(\frac{E}{E^*} - \frac{I}{I^*}\right)\right] \\
&= \lambda^* S^*\left(1 - \frac{I^*}{I}\right)\left(\frac{E}{E^*} - \frac{I}{I^*}\right) \\
&= \lambda^* S^*\left(1 - \frac{I}{I^*} - \frac{EI^*}{E^* I} + \frac{E}{E^*}\right).
\end{aligned} \tag{3.48}$$

Using $\dot{T} = \kappa I - (\alpha_2 + \Psi + \mu)T$ and the equilibrium relation (3.45), we have

$$\begin{aligned}
\dot{L}_T &= \frac{W_T \lambda^* S^*}{\kappa I^*}\left(1 - \frac{T^*}{T}\right)\dot{T} \\
&= \frac{W_T \lambda^* S^*}{\kappa I^*}\left(1 - \frac{T^*}{T}\right)\left(\kappa I - \frac{\kappa I^*}{T^*} T\right) \\
&= \frac{W_T \lambda^* S^*}{\kappa I^*}\left[\kappa I^*\left(1 - \frac{T^*}{T}\right)\left(\frac{I}{I^*} - \frac{T}{T^*}\right)\right] \\
&= W_T \lambda^* S^*\left(1 - \frac{T^*}{T}\right)\left(\frac{I}{I^*} - \frac{T}{T^*}\right) \\
&= W_T \lambda^* S^*\left(1 - \frac{T}{T^*} - \frac{IT^*}{I^* T} + \frac{I}{I^*}\right).
\end{aligned} \tag{3.49}$$

Summing $\dot{L} = \dot{L}_S + \dot{L}_E + \dot{L}_I + \dot{L}_T$, the terms $\pm\frac{\lambda S}{\lambda^* S^*}$ and $\pm\frac{E}{E^*}$ cancel. Collecting the remaining terms, we have

$$\begin{aligned}
\dot{L} = -\mu\frac{(S - S^*)^2}{S} + \lambda^* S^*\left[3 - \frac{S^*}{S} - \frac{I}{I^*} - \frac{EI^*}{E^* I} - \frac{\lambda S E^*}{\lambda^* S^* E} + \frac{\lambda}{\lambda^*}\right] \\
+ W_T \lambda^* S^*\left(1 - \frac{T}{T^*} - \frac{IT^*}{I^* T} + \frac{I}{I^*}\right).
\end{aligned} \tag{3.50}$$

Using Lemma 1, we substitute $\frac{\lambda}{\lambda^*} = W_I\frac{I}{I^*} + W_T\frac{T}{T^*}$ and multiply the terms $\left(3, \frac{S}{S^*}, \frac{I}{I^*}, \frac{EI^*}{E^* I}\right)$ by $(W_I + W_T) = 1$ as follows:

$$\begin{aligned}
\dot{L} = -\mu\frac{(S - S^*)^2}{S} + W_I \lambda^* S^*\left[\frac{I}{I^*} - \frac{S E^* I}{S^* E I^*}\right] + W_T \lambda^* S^*\left[\frac{T}{T^*} - \frac{S E^* T}{S^* E T^*}\right] \\
+ W_I \lambda^* S^*\left[3 - \frac{S^*}{S} - \frac{I}{I^*} - \frac{EI^*}{E^* I}\right] \\
+ W_T \lambda^* S^*\left[3 - \frac{S^*}{S} - \frac{I}{I^*} - \frac{EI^*}{E^* I}\right]
\end{aligned}$$

$$+ W_T\lambda^* S^* \left[1 - \frac{T}{T^*} - \frac{IT^*}{I^*T} + \frac{I}{I^*}\right]. \tag{3.51}$$

Expanding the sum and grouping by the weights $W_I\lambda^* S^*$ and $W_T\lambda^* S^*$, the terms $\pm\frac{I}{I^*}$ and $\pm\frac{T}{T^*}$ cancel. We obtain

$$\begin{aligned}\dot{L} = &-\mu\frac{(S - S^*)^2}{S} \\ &+ W_I\lambda^* S^* \left[3 - \frac{S^*}{S} - \frac{EI^*}{E^*I} - \frac{SE^*I}{S^*EI^*}\right] \\ &+ W_T\lambda^* S^* \left[4 - \frac{S^*}{S} - \frac{EI^*}{E^*I} - \frac{IT^*}{I^*T} - \frac{SE^*T}{S^*ET^*}\right].\end{aligned} \tag{3.52}$$

By the AM–GM inequality, the expressions in the W_I and W_T brackets are nonpositive because the product of the ratios in each bracket equals one. Hence, $\dot{L} \le 0$ in the positive interior of Ω^*.

We now identify the largest invariant set contained in $\{\dot{L} = 0\}$. Equality in the AM–GM inequalities implies

$$S = S^*, \qquad \frac{E}{E^*} = \frac{I}{I^*} = \frac{T}{T^*}.$$

Let this common ratio be $c > 0$. On the largest invariant set contained in $\{\dot{L} = 0\}$, the susceptible equation satisfies

$$0 = \dot{S} = \Pi - \lambda S - \mu S.$$

Using $\delta = 0$, $S = S^*$, $\lambda = c\lambda^*$, and the equilibrium relation

$$\Pi = \lambda^* S^* + \mu S^*,$$

we obtain

$$0 = (1 - c)\lambda^* S^*.$$

Since $\lambda^* S^* > 0$, it follows that $c = 1$. Therefore on the largest invariant set,

$$S = S^*, \qquad E = E^*, \qquad I = I^*, \qquad T = T^*.$$

Moreover, since $T = T^*$, the equation for F becomes

$$\frac{d}{dt}(F - F^*) = -(\alpha_3 + \mu)(F - F^*).$$

Invariance and boundedness in Ω^* therefore require $F = F^*$. Since $N = N^*$, it then follows that

$$R = N^* - S - E - I - T - F = R^*.$$

Thus, the largest invariant set contained in $\{\dot{L} = 0\}$ is $\{P^*\}$. By LaSalle's invariance principle, every solution in the interior of Ω^* converges to P^*. Therefore, P^* is globally asymptotically stable in the interior of the reduced feasible region Ω^* whenever $\delta = 0$, $N = N^*$, and $\mathcal{R}_0 > 1$. □

The preceding results identify the threshold at which the DFE changes stability and a positive EE emerges. Because the EE stability statements are obtained under the stated reductions, the following proposition is understood as a local bifurcation statement at the DFE.

Proposition 1. *System* (2.2) *undergoes a forward transcritical bifurcation at* $\mathcal{R}_0 = 1$. *The DFE* P_0 *is stable below the threshold and loses stability as* $\mathcal{R}_0$ *crosses one, while a positive EE emerges for* $\mathcal{R}_0 > 1$.

4. Sensitivity analysis

Sensitivity analysis is an important component of epidemiological studies because it quantifies the relative importance of each model parameter in determining the magnitude of the basic reproduction number $\mathcal{R}_0$. Identifying these key drivers allows public health interventions to be prioritized effectively. The normalized sensitivity index for a given parameter p is defined as

$$\Upsilon_p^{\mathcal{R}_0} = \frac{\partial \mathcal{R}_0}{\partial p} \times \frac{p}{\mathcal{R}_0}. \tag{4.1}$$

Given the explicit expression for $\mathcal{R}_0$ established in Theorem 5, the sensitivity indices for the core parameters are computed as follows. Because $\mathcal{R}_0$ is linearly proportional to the transmission coefficient β, we have

$$\Upsilon_\beta^{\mathcal{R}_0} = 1. \tag{4.2}$$

This confirms that $\mathcal{R}_0$ increases with β, and reducing the transmission rate through hygiene and social distancing remains the most direct method of disease control. For the progression rate Φ, which represents the rate of transition from latent to infectious, we obtain

$$\Upsilon_\Phi^{\mathcal{R}_0} = \frac{\mu}{\Phi + \mu} > 0. \tag{4.3}$$

This positive index shows that $\mathcal{R}_0$ increases with Φ, indicating that a faster transition to the infectious stage accelerates disease spread.

For the natural recovery rate α_1 and the treatment recovery rate α_2, we obtain

$$\Upsilon_{\alpha_1}^{\mathcal{R}_0} = -\frac{\alpha_1}{\alpha_1 + \kappa + \mu} < 0, \quad \Upsilon_{\alpha_2}^{\mathcal{R}_0} = -\frac{\alpha_2}{\alpha_2 + \Psi + \mu} \cdot \frac{\epsilon\kappa}{\alpha_2 + \Psi + \mu + \epsilon\kappa} < 0. \tag{4.4}$$

Both indices are strictly negative, implying that $\mathcal{R}_0$ decreases as recovery rates increase. This demonstrates that therapeutic interventions that accelerate recovery can substantially reduce disease transmission. Furthermore, for the modification factor ϵ, which accounts for the relative infectiousness of treated individuals, we obtain

$$\Upsilon_\epsilon^{\mathcal{R}_0} = \frac{\epsilon\kappa}{\alpha_2 + \Psi + \mu + \epsilon\kappa} > 0. \tag{4.5}$$

The positive sign highlights that the continued infectiousness of treated individuals is a risk factor for disease persistence; as ϵ increases, so does $\mathcal{R}_0$.

The effect of the treatment initiation rate κ requires more care. Differentiating both sides of (3.2) with respect to κ gives

$$\frac{\partial \mathcal{R}_0}{\partial \kappa} = \frac{\beta\Phi}{(\Phi + \mu)(\alpha_2 + \Psi + \mu)} \frac{\epsilon(\alpha_1 + \mu) - (\alpha_2 + \Psi + \mu)}{(\alpha_1 + \kappa + \mu)^2}. \tag{4.6}$$

Consequently, we have

$$\Upsilon_\kappa^{\mathcal{R}_0} = \frac{\kappa\left[\epsilon(\alpha_1 + \mu) - (\alpha_2 + \Psi + \mu)\right]}{(\alpha_1 + \kappa + \mu)(\alpha_2 + \Psi + \mu + \epsilon\kappa)}. \tag{4.7}$$

Thus, increasing the treatment rate decreases $\mathcal{R}_0$ if

$$\epsilon(\alpha_1 + \mu) < \alpha_2 + \Psi + \mu, \tag{4.8}$$

and increases $\mathcal{R}_0$ if

$$\epsilon(\alpha_1 + \mu) > \alpha_2 + \Psi + \mu. \tag{4.9}$$

Equivalently, the critical residual infectiousness level is

$$\epsilon_\kappa^* = \frac{\alpha_2 + \Psi + \mu}{\alpha_1 + \mu}. \tag{4.10}$$

If $\epsilon < \epsilon_\kappa^*$, faster treatment is beneficial; if $\epsilon > \epsilon_\kappa^*$, treatment can increase the reproduction number because it moves individuals into a treated class that remains sufficiently infectious for long enough to generate additional cases. Since $0 \le \epsilon \le 1$, the risk case can occur only when $\alpha_2 + \Psi + \mu < \alpha_1 + \mu$; that is, when the exit rate from the treated class is lower than that from the untreated infectious class and residual infectiousness during treatment is high. This condition gives a clear public-health interpretation: Increasing treatment speed is safe only when the treatment is coupled with rapid recovery, effective isolation, or a strong reduction in infectiousness.

The isolated failure assumption can also be checked analytically by allowing a second modification factor for failed treatment cases. For the auxiliary force of infection in (3.4), the sensitivity of $\mathcal{R}_0^F$ given in (3.5) with respect to ϵ_F, is given by

$$\Upsilon_{\epsilon_F}^{\mathcal{R}_0^F} = \frac{\dfrac{\epsilon_F \Psi \kappa}{(\alpha_2 + \Psi + \mu)(\alpha_3 + \mu)}}{1 + \dfrac{\epsilon\kappa}{\alpha_2 + \Psi + \mu} + \dfrac{\epsilon_F \Psi \kappa}{(\alpha_2 + \Psi + \mu)(\alpha_3 + \mu)}} \ge 0. \tag{4.11}$$

Therefore, any residual infectiousness in F increases the threshold quantity. The main model uses $\epsilon_F = 0$, which represents complete removal of failed treatment cases from effective transmission; if field data show that failed treatment individuals continue to mix, then the auxiliary expression $\mathcal{R}_0^F$ should be used instead of the main $\mathcal{R}_0$.

From a public health perspective, these results suggest a hierarchical approach to intervention. Minimizing parameters with positive indices (β, Φ, ϵ, and, in the auxiliary model, ϵ_F) and maximizing those with negative indices (α_1, α_2) are essential to driving $\mathcal{R}_0$ below unity. Treatment initiation should be paired with reduced contact and rapid clinical resolution; otherwise, its effect can be weakened or, under Condition (4.9), reversed.

5. Bifurcation analysis

The stability results indicate that a threshold transition occurs at $\mathcal{R}_0 = 1$. We take the transmission rate β as the bifurcation parameter.

Theorem 11. *At $\beta = \beta_c$, System (2.2) undergoes a forward transcritical bifurcation at the DFE P_0. The DFE is locally asymptotically stable in Ω for $\beta \le \beta_c$ and unstable for $\beta > \beta_c$, while a positive endemic branch exists for $\beta > \beta_c$.*

Proof. We use the center manifold framework of Castillo-Chavez and Song [38]. At

$$P_0 = \left(\frac{\Pi}{\mu}, 0, 0, 0, 0, 0\right) \qquad \text{and} \qquad \beta = \beta_c,$$

the Jacobian matrix (3.6) has the block structure described in Theorem 6. As established in the proof of Theorem 7, zero is a simple eigenvalue of $J(P_0, \beta_c)$, while all its remaining eigenvalues have negative real parts.

Let q and p denote the full right and left zero eigenvectors constructed in the proof of Theorem 7, using the state ordering

$$\mathcal{X} = (S, E, I, T, F, R)^\top.$$

From (3.10)–(3.13), their components satisfy

$$q_I = 1, \qquad q_T = \frac{\kappa}{d_3}, \qquad q_S = \eta_S < 0, \qquad p_E = \omega,$$

where ω is given in (3.11). Moreover, we have

$$J(P_0, \beta_c)q = 0, \qquad p^\top J(P_0, \beta_c) = 0, \qquad p^\top q = 1.$$

On the center manifold, the local dynamics have the normal form

$$\dot{w} = b(\beta - \beta_c)w + \frac{1}{2}aw^2 + O\left(|w|^3 + |\beta - \beta_c|\,|w|^2 + |\beta - \beta_c|^2|w|\right). \tag{5.1}$$

Following the standard center manifold notation, the coefficients are

$$a = \sum_{k=1}^{6}\sum_{i=1}^{6}\sum_{j=1}^{6} p_k q_i q_j \frac{\partial^2 f_k}{\partial \mathcal{X}_i \partial \mathcal{X}_j}(P_0, \beta_c),$$

and

$$b = \sum_{k=1}^{6}\sum_{i=1}^{6} p_k q_i \frac{\partial^2 f_k}{\partial \mathcal{X}_i \partial \beta}(P_0, \beta_c).$$

In System (2.2), all transition, recovery, treatment, failure, recruitment, and mortality terms are linear. Therefore, the only nonzero second derivatives arise from the standard incidence transmission term. This term appears with opposite signs in the S- and the E-equations. Since $p_S = 0$, the contribution from the S-equation vanishes. Hence, only the E-equation contributes to a and b.

The contraction defining a is exactly the threshold coefficient ℓ calculated in (3.15). Indeed, since $p_E = \omega$, $q_S = \eta_S$, and $q_I + \epsilon q_T = 1 + \epsilon\kappa/d_3$, we have

$$\begin{aligned} a &= \frac{2\beta_c\omega}{N^0}(q_I + \epsilon q_T)q_S \\ &= \frac{2\beta_c\omega}{N^0}\left(1 + \frac{\epsilon\kappa}{d_3}\right)\eta_S \\ &= \ell < 0. \end{aligned}$$

Next, for the coefficient b, the only nonzero mixed state-parameter derivatives of the E-equation are

$$\frac{\partial^2 f_2}{\partial I \partial \beta}(P_0, \beta_c) = 1, \qquad \frac{\partial^2 f_2}{\partial T \partial \beta}(P_0, \beta_c) = \epsilon.$$

Therefore, we have

$$\begin{aligned} b &= p_E \sum_{i=1}^{6} q_i \frac{\partial^2 f_2}{\partial \mathcal{X}_i \partial \beta}(P_0, \beta_c) \\ &= p_E(q_I + \epsilon q_T) \\ &= \omega \left(1 + \frac{\epsilon \kappa}{d_3}\right) > 0. \end{aligned}$$

Thus

$$a < 0, \qquad b > 0.$$

By setting $\dot{w} = 0$ in (5.1), the equilibria of the reduced system satisfy

$$0 = b\,(\beta - \beta_c)\, w + \frac{1}{2} a w^2 + O\left(|w|^3 + |\beta - \beta_c|\,|w|^2 + |\beta - \beta_c|^2 |w|\right).$$

The corresponding leading-order bifurcation equation is

$$w\left(b\,(\beta - \beta_c) + \frac{1}{2} a w\right) = 0.$$

Thus, in addition to the DFE branch $w = 0$, there is a nontrivial equilibrium branch satisfying

$$w_* = -\frac{2b}{a}(\beta - \beta_c) + O\left(|\beta - \beta_c|^2\right).$$

Since $a < 0$ and $b > 0$, the leading term of w_* is positive for $\beta > \beta_c$. Therefore, a positive EE branch emerges on the side $\beta > \beta_c$, and the bifurcation is forward transcritical. Moreover, the stability statements for the DFE follow from Theorems 6 and 7: The DFE is locally asymptotically stable in Ω for $\beta \le \beta_c$ and unstable for $\beta > \beta_c$. □

The forward nature of the bifurcation has a useful epidemiological interpretation. In the model considered here, reducing $\mathcal{R}_0$ below one removes the locally stable endemic branch near the threshold. Thus, interventions that lower contact, reduce residual infectiousness during treatment, or shorten infectious periods directly support elimination.

6. Numerical simulations

This section presents numerical simulations illustrating the analytical results for System (2.2). All parameters are expressed on a per-day basis, consistent with the short incubation and recovery timescales of conjunctival infections. Baseline values are listed in Table 2.

Table 2. Baseline parameter values for System (2.2).

Parameter	Numerical value	Unit	Primary source
Π	0.056	day^{-1}	[39]
μ	0.00004	day^{-1}	[11]
β	0.35	day^{-1}	[13]
ϵ	0.05	–	[14]
Φ	0.25	day^{-1}	[2]
κ	0.15	day^{-1}	[39]
Ψ	0.02	day^{-1}	[17]
α_1	0.14	day^{-1}	[13]
α_2	0.30	day^{-1}	[39]
α_3	0.20	day^{-1}	Assumed baseline
δ	0.001	day^{-1}	[12]

The parameters values come from conjunctivitis or closely related epidemic modeling studies where available. Parameters for which direct conjunctivitis-specific estimates are unavailable are used as the baseline scenario values and interpreted alongside the sensitivity analysis. The natural death rate $\mu = 0.00004$ corresponds to an average life expectancy of approximately 68 years, while $\delta = 0.001$ corresponds to an average duration of temporary immunity of approximately 1000 days. The recovery parameters distinguish natural and treated recovery: $\alpha_1 = 0.14$ gives an average untreated infectious period of about 7.1 days, whereas $\alpha_2 = 0.30$ gives an average treated duration of about 3.3 days when competing exits are ignored. The treatment failure parameter $\Psi = 0.02\ \text{day}^{-1}$ is used as a daily transition rate from treated individuals to the failure class. It should not be interpreted as a cumulative probability over the entire treatment period. In the model, the probability that a treated individual eventually enters the failed treatment class is

$$\frac{\Psi}{\alpha_2 + \Psi + \mu},$$

because recovery and natural mortality compete with treatment failure.

The simulations are not empirically calibrated to a specific outbreak. Data from the 2003 acute hemorrhagic conjunctivitis outbreak in Mexico have been analyzed previously; for example, clinical records from Colima included 886 cases during September–November 2003, with an epidemic peak around late September and an estimated reproduction number of approximately four in related analyses [11, 40]. However, those data do not resolve the treated and failed treatment compartments required for direct estimation of κ, Ψ, α_2, α_3, ϵ, and ϵ_F. A full calibration would require an observation model and time-series information on treatment initiation, treatment failure, recovery, and isolation behavior. The numerical results below are scenario-based illustrations of the analytical thresholds and stability properties.

All simulations and figures were generated in `Python`. Time-dependent solutions of the SEITFR system were computed using `solve_ivp` from `SciPy`. Standard time-series solutions were computed using the adaptive Runge–Kutta method `RK45`, whereas long-time solutions with slow convergence were computed using the implicit `BDF` method. Relative tolerances between 10^{-8} and 10^{-9} and absolute tolerances between 10^{-10} and 10^{-12} were used.

6.1. Numerical stability analysis

We first illustrate the threshold behavior predicted by the stability results. Using the baseline parameter values in Table 2 and applying (3.8), we obtain

$$\beta_c \approx 0.284.$$

In Figure 2, the transmission rate β is varied according to the relation

$$\beta = \mathcal{R}_0 \beta_c \tag{6.1}$$

to produce seven prescribed values of $\mathcal{R}_0$. For $\mathcal{R}_0 < 1$, the infectious compartments decay toward zero and the solution approaches the DFE. For $\mathcal{R}_0 > 1$, the solution approaches positive endemic levels through damped transient oscillations. Note that the initial conditions in this simulation were chosen so that

$$N(0) = S(0) + E(0) + I(0) + T(0) + F(0) + R(0) = N^* = \frac{\Pi}{\mu} = 1400.$$

Since the total population satisfies (2.4) for all t, $N(t)$ remains fixed for all prescribed values of $\mathcal{R}_0$, as shown in Figure 2(g).

To complement the threshold simulations in Figure 2, we also examine the critical case $\mathcal{R}_0 = 1$. Using the baseline parameter values in Table 2 and setting $\beta = \beta_c$, the system was simulated from the initial condition

$$(S(0), E(0), I(0), T(0), F(0), R(0)) = (1300, 20, 20, 20, 20, 20),$$

for which $N(0) = N^0 = \Pi/\mu = 1400$. Since the DFE is nonhyperbolic at the critical threshold, convergence is expected to be slower than in the strictly subthreshold case $\mathcal{R}_0 < 1$. For this reason, the simulation interval was extended to 8000 days.

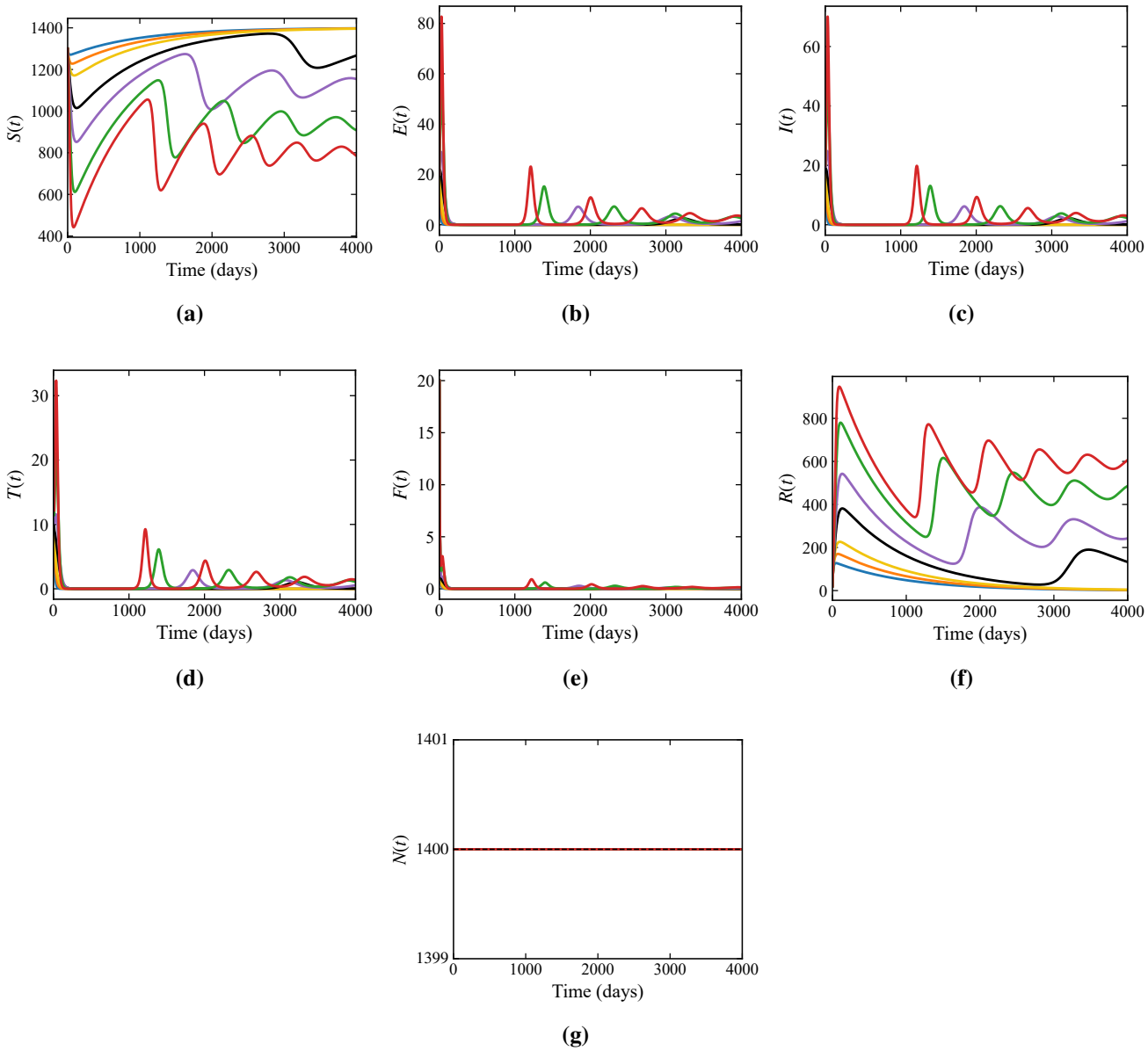

Figure 2. Numerical simulation of System (2.2) for different values of $\mathcal{R}_0$. Blue: $\mathcal{R}_0 = 0.50$; orange: $\mathcal{R}_0 = 0.75$; yellow: $\mathcal{R}_0 = 0.9$; black: $\mathcal{R}_0 = 1.1$; purple: $\mathcal{R}_0 = 1.25$; green: $\mathcal{R}_0 = 1.50$; red: $\mathcal{R}_0 = 1.75$. The DFE is approached for $\mathcal{R}_0 < 1$, whereas damped convergence toward positive endemic levels occurs for $\mathcal{R}_0 > 1$.

Figure 3(a) shows that the susceptible population approaches its DFE value $S^0 = \Pi/\mu = 1400$. Figure 3(b) shows that the exposed, infectious, treated, treatment failure, and recovered compartments gradually decay toward zero. To display the convergence of the full state vector, Figure 3(c) plots the distance

$$D(t) = \|\mathbf{U}(t) - P_0\|_1, \qquad \mathbf{U}(t) = (S(t), E(t), I(t), T(t), F(t), R(t))^\top.$$

The gradual decay of $D(t)$ toward zero is consistent with the loss of hyperbolicity at $\mathcal{R}_0 = 1$ and numerically supports the local asymptotic stability result established in Theorem 7.

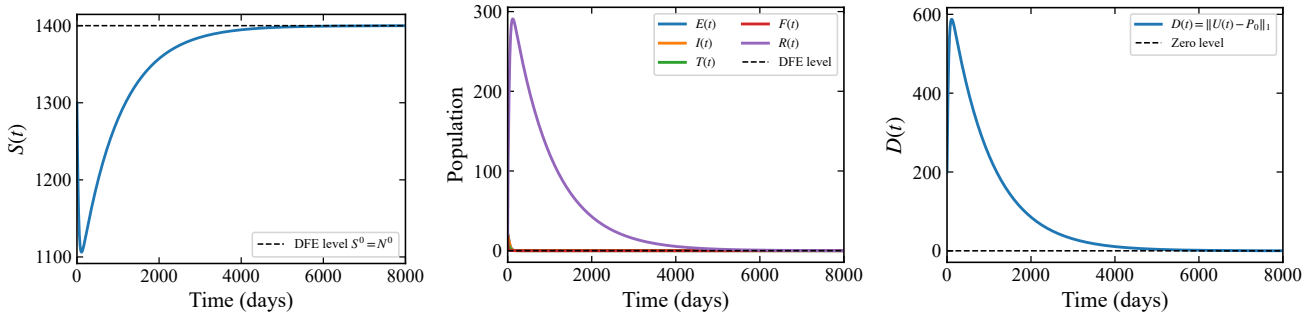

(a) **(b)** **(c)**

Figure 3. Numerical stability analysis at the critical threshold $\mathcal{R}_0 = 1$, with $\beta = \beta_c$. (a) Time evolution of the susceptible compartment $S(t)$, with the dashed line indicating the DFE value $S^0 = N^0 = \Pi/\mu$. (b) Time evolution of the nonsusceptible compartments $E(t)$, $I(t)$, $T(t)$, $F(t)$, and $R(t)$, which approach zero. (c) The distance $D(t) = \|\mathbf{U}(t) - P_0\|_1$ between the numerical solution and the DFE. The slow convergence reflects the nonhyperbolic character of the critical case and supports Theorem 7.

The damped approach to the endemic state is further illustrated in the phase-plane plots in Figure 4. The inward spirals in the (S, I) and (R, I) planes indicate stable focus behavior for the selected endemic parameter set. This is consistent with the occurrence of complex conjugate eigenvalues with negative real parts.

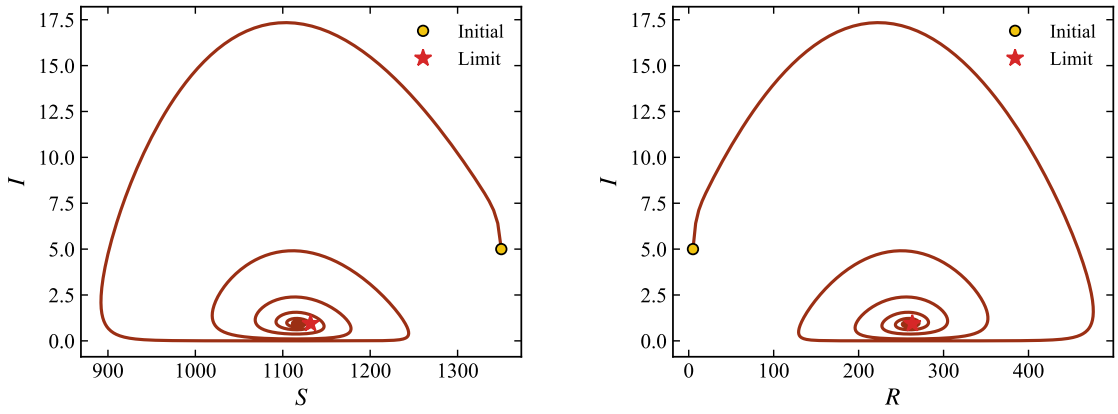

(a) **(b)**

Figure 4. Phase-plane trajectories for a representative endemic case. The inward spirals in the (S, I) and (R, I) planes illustrate stable focus convergence toward the endemic state.

We next illustrate the global stability result for the DFE. For this test, we set $\mathcal{R}_0 = 0.65 < 1$ and simulate four different non-negative initial conditions. Figure 5 shows that all trajectories converge to

$$P_0 = (1400, 0, 0, 0, 0, 0)\,.$$

The infected compartments vanish for all initial conditions, illustrating the global stability of the DFE.

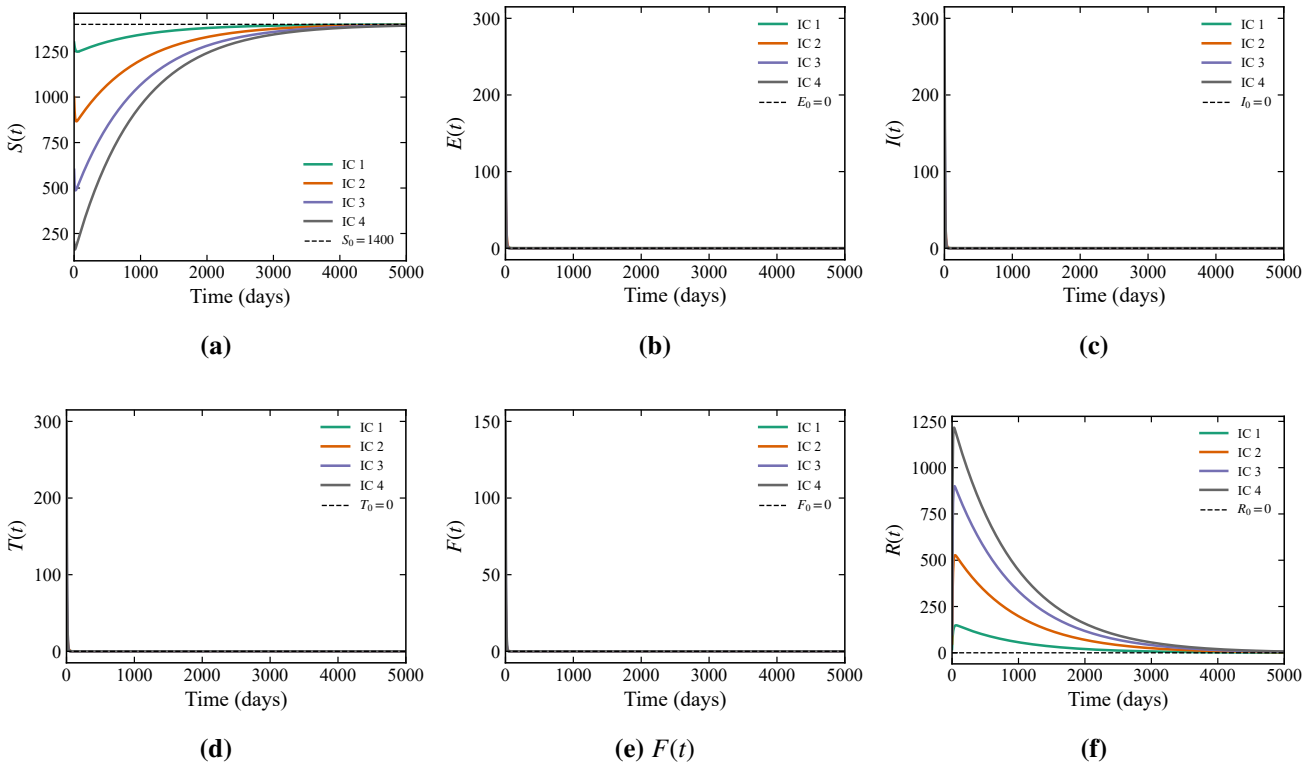

Figure 5. Global stability of the DFE for $\mathcal{R}_0 = 0.65 < 1$. Four different non-negative initial conditions converge to the DFE $P_0 = (\Pi/\mu, 0, 0, 0, 0, 0)$. The dashed black line marks the corresponding DFE value in each panel. The infected compartments vanish, while $S(t)$ approaches $\Pi/\mu = 1400$.

We next illustrate the global stability result for the EE under the assumptions of Theorem 10. For this test, we set $\delta = 0$, impose $N(0) = N^* = 1400$, and choose $\mathcal{R}_0 = 1.20 > 1$. Substituting these values into the EE formula derived in Theorem 9 gives

$$P^* = (1166.667,\ 0.0373,\ 0.0322,\ 0.0151,\ 0.0015,\ 233.247).$$

Since the natural death rate $\mu = 0.00004$ is very small, convergence to the EE occurs on a long time scale. The dominant eigenvalues near P^* are approximately

$$\sigma_{1,2} \approx -2.30 \times 10^{-5} \pm 1.03 \times 10^{-3} i,$$

corresponding to an oscillation period of about 6.1×10^3 days and an exponential decay time of about 4.35×10^4 days. Therefore, a long simulation interval was used to display the slow damped convergence. Figure 6 shows that the trajectories of all six compartments converge to the analytically computed equilibrium P^*, thereby supporting the global stability result under the stated assumptions and confirming the correctness of the EE formula in Theorem 9.

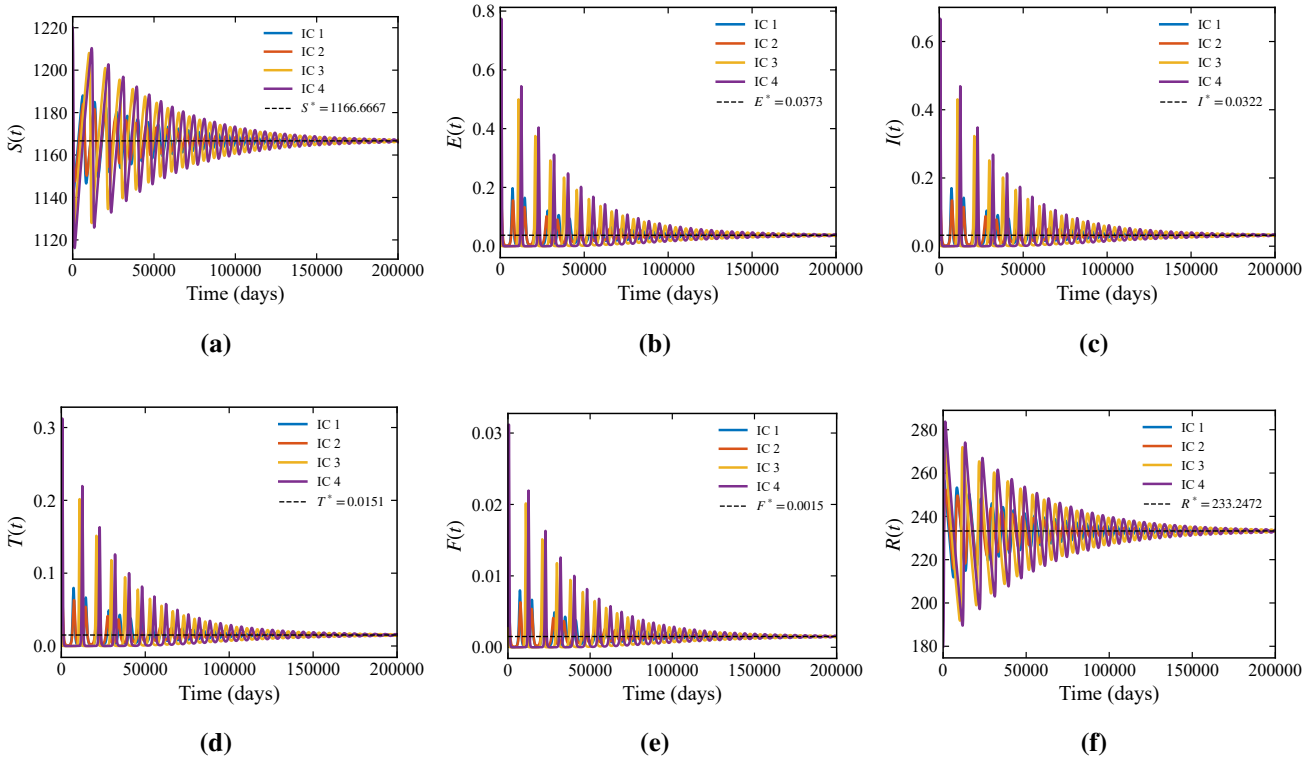

Figure 6. Convergence to the EE for $\mathcal{R}_0 = 1.20$ under the assumptions $\delta = 0$ and $N(0) = N^*$. The dashed black line marks the corresponding EE value in each compartment. The long simulation interval is used because the dominant eigenvalues near P^* have small negative real parts, producing slow damped convergence.

To complement the analytical stability results, we also performed a numerical local stability test for the EE using the baseline parameter values in Table 2. The analytical global stability result for the EE was proved under the simplifying assumption $\delta = 0$, whereas the baseline numerical value is $\delta = 0.001$. Therefore, for the baseline parameter setting, we evaluated the eigenvalues of the full Jacobian matrix $J(P^*)$ at the EE.

For each value of $\mathcal{R}_0$ in the interval

$$1.01 \leq \mathcal{R}_0 \leq 2.50,$$

with step size 0.01, the transmission rate was chosen as (6.1). All remaining parameters were fixed at their baseline values. For each resulting EE P^*, the eigenvalues σ_i of the full Jacobian matrix $J(P^*)$ were computed, and the quantity

$$\max_i \mathrm{Re}(\sigma_i)$$

was recorded. As shown in Figure 7, this quantity remains below zero throughout the tested interval, confirming the numerical local asymptotic stability of the EE for $1.01 \leq \mathcal{R}_0 \leq 2.50$.

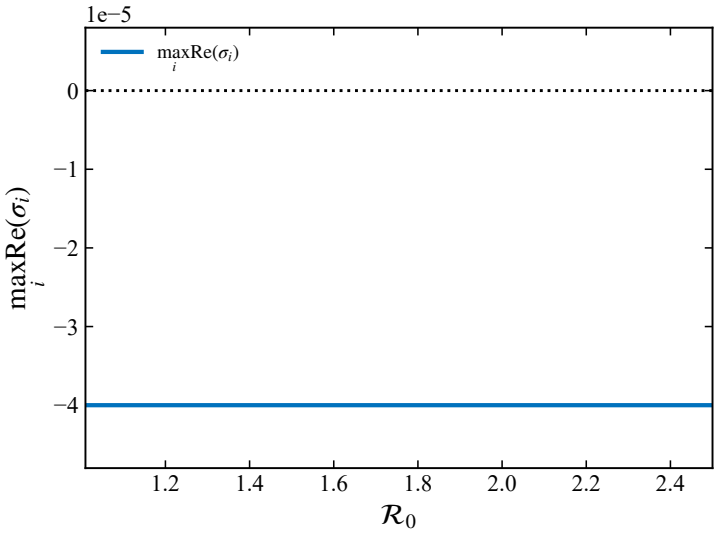

Figure 7. Numerical local stability test of the EE P^* for $1.01 \leq \mathcal{R}_0 \leq 2.50$. For each value of $\mathcal{R}_0$, the transmission rate was set as (6.1), while the remaining parameters were fixed at their baseline values in Table 2. The plotted quantity is $\max_i \mathrm{Re}(\sigma_i)$, where σ_i are the eigenvalues of the full Jacobian matrix evaluated at P^*.

In this numerical test, the dominant eigenvalue of the full Jacobian matrix $J(P^*)$ was numerically found to satisfy

$$\max_i \mathrm{Re}(\sigma_i) = -\mu = -4 \times 10^{-5}.$$

The fact that $-\mu$ is an eigenvalue follows from the equation for the total population derived earlier in (2.4). Indeed, if $\boldsymbol{v} = (1, 1, 1, 1, 1, 1)^\top$, then

$$\boldsymbol{v}^\top J(P^*) = -\mu \boldsymbol{v}^\top.$$

Thus, $\boldsymbol{v}^\top$ is a left eigenvector of $J(P^*)$ associated with the eigenvalue $-\mu$. Over the tested range $1.01 \leq \mathcal{R}_0 \leq 2.50$, all remaining eigenvalues were numerically found to have real parts smaller than $-\mu$. Hence, all eigenvalues remain in the open left half-plane, supporting the numerical local asymptotic stability of the EE under the baseline parameter setting.

6.2. Sensitivity analysis

The sensitivity indices and the one- and two-parameter plots were computed directly from the analytical expression for $\mathcal{R}_0$. In the one-parameter and two-parameter plots, only the indicated parameter or parameter pair was varied; all remaining parameters were fixed at their baseline values in Table 2.

Figure 8 shows that β has the largest positive effect, with an index of +1. At the baseline parameter values, κ has a negative sensitivity index because Condition (4.8) holds, so faster treatment reduces $\mathcal{R}_0$. This effect is conditional: If treated individuals remain sufficiently infectious, as described by (4.9), increasing κ could instead increase $\mathcal{R}_0$.

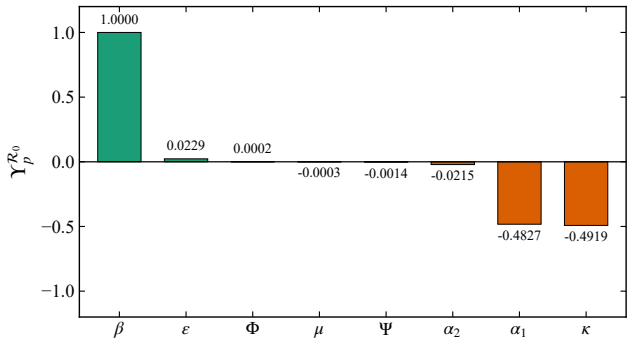

Figure 8. Normalized sensitivity indices of $\mathcal{R}_0$ evaluated at the baseline parameter values. Positive indices indicate parameters that increase $\mathcal{R}_0$, while negative indices indicate parameters that reduce $\mathcal{R}_0$.

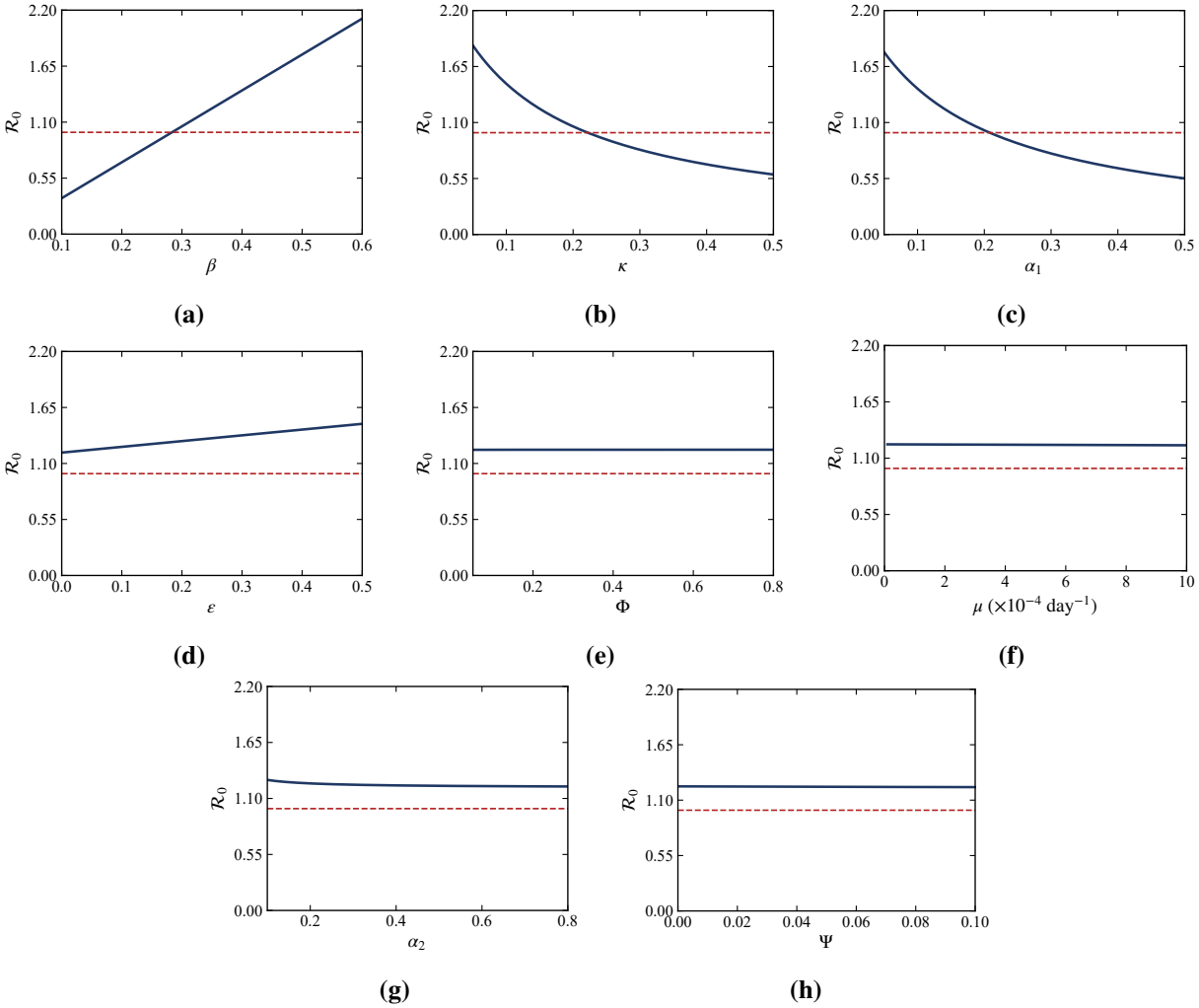

Figure 9. One-parameter impact plots showing how $\mathcal{R}_0$ changes when each parameter is varied around the baseline value while the remaining parameters are fixed. The red dashed line marks $\mathcal{R}_0 = 1$. All figures use the same vertical scale to allow direct comparison. In Figure 9f, the horizontal axis is displayed as $10^4\mu$ to avoid very small tick labels.

Figure 9 confirms these rankings through one-parameter sweeps. The transmission rate β increases $\mathcal{R}_0$ linearly, while increasing α_1 lowers it. At the baseline, the effect of κ is beneficial because treated individuals have low residual infectiousness. The parameters α_2 and Ψ have smaller baseline effects because they act only after individuals enter treatment.

Figure 10 shows the combined effects of selected parameter pairs. The red dashed curves mark $\mathcal{R}_0 = 1$ and separate the disease elimination region from the persistence region. In the (β, κ) plane, increasing κ lowers $\mathcal{R}_0$ under the baseline residual infectiousness $\epsilon = 0.05$, but high transmission still requires a reduction in β. The (β, α_1) and (α_1, κ) panels show that faster recovery and faster effective treatment expand the elimination region. Overall, the contour plots support combined interventions that reduce transmission and improve clinical resolution while ensuring that treatment reduces effective infectiousness.

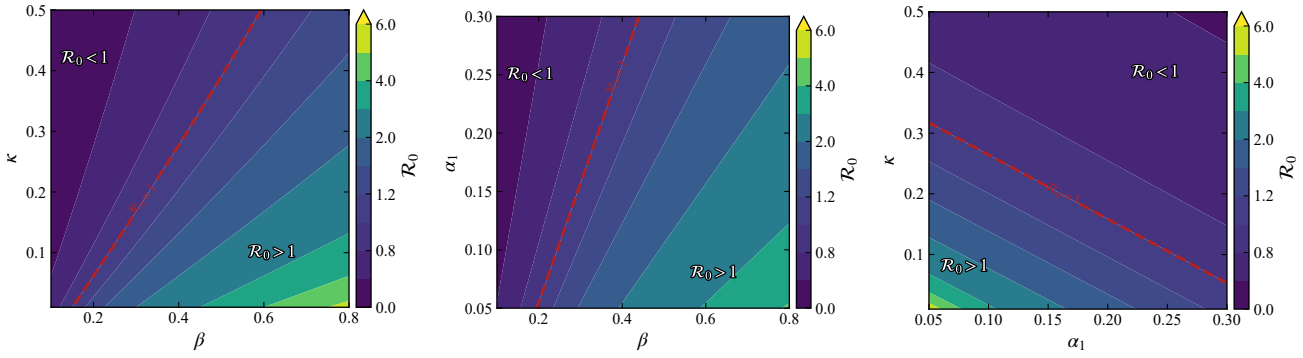

Figure 10. Two-parameter contour plots of $\mathcal{R}_0$ around the baseline parameter set. The red dashed curve marks the threshold $\mathcal{R}_0 = 1$, separating the disease elimination region ($\mathcal{R}_0 < 1$) from the persistence region ($\mathcal{R}_0 > 1$). Increasing β shifts the system toward larger $\mathcal{R}_0$, whereas increasing α_1 or κ moves the system toward lower $\mathcal{R}_0$ under the baseline condition (4.8).

6.3. Numerical bifurcation analysis

Finally, Figure 11 illustrates the bifurcation diagram of the steady-state infectious class I^* with respect to β. The diagram was computed directly from the analytical equilibrium expression, not from time integration. The critical value (3.8) is $\beta_c \approx 0.284$, where $\mathcal{R}_0 = 1$. The DFE is stable for $\beta < \beta_c$ and unstable for $\beta > \beta_c$, while a locally stable endemic branch emerges for $\beta > \beta_c$ near the threshold. The diagram is consistent with the forward transcritical bifurcation derived analytically.

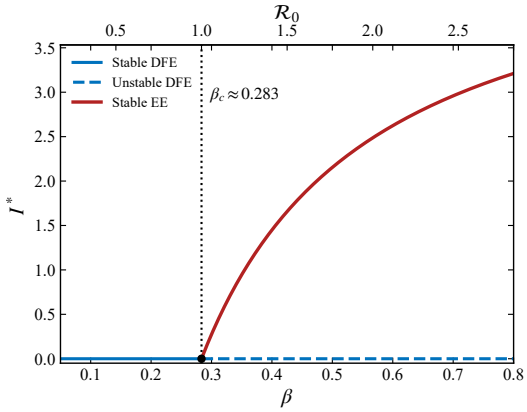

Figure 11. Forward transcritical bifurcation with respect to the transmission rate β. The DFE is stable for $\beta < \beta_c$ and unstable for $\beta > \beta_c$, while a locally stable EE branch emerges for $\beta > \beta_c$ near the threshold. The vertical dashed line marks $\beta_c \approx 0.284$, where $\mathcal{R}_0 = 1$.

7. Conclusions

We developed and analyzed an SEITFR model for conjunctivitis transmission with treatment, reduced infectiousness during treatment, and detected treatment failure. A key clarification in the revised formulation is that the residual transmission reservoir is the treated class T, whose contribution to transmission is scaled by ϵ. The failed treatment class F represents detected cases that are assumed to be isolated, referred for further care, or otherwise removed from effective community transmission; therefore, F is not included in the force of infection.

The model is mathematically well-posed in the feasible region: The solutions remain non-negative, bounded, and unique. The basic reproduction number $\mathcal{R}_0$ was derived using the next-generation matrix method and decomposed into the transmission contributions of I and the partially infectious class T. The DFE is locally asymptotically stable for $\mathcal{R}_0 \leq 1$, globally asymptotically stable for $\mathcal{R}_0 < 1$, and unstable for $\mathcal{R}_0 > 1$. A unique positive EE exists when $\mathcal{R}_0 > 1$. Its global stability was proved under the additional assumptions of a constant total population ($N = N^*$) and no loss of immunity ($\delta = 0$). For the baseline loss of immunity rate used in the numerical simulations, the local stability of the EE was further supported by eigenvalue computations of the full Jacobian matrix.

The center manifold analysis shows that the model undergoes a forward transcritical bifurcation at $\mathcal{R}_0 = 1$. Thus, in the present isolated failure setting, crossing the threshold creates a locally stable endemic branch in the forward direction near the threshold, rather than a backward bifurcation scenario. The sensitivity analysis gives a precise condition for the effect of treatment initiation: Increasing κ reduces $\mathcal{R}_0$ when $\epsilon(\alpha_1 + \mu) < \alpha_2 + \Psi + \mu$, but it can increase $\mathcal{R}_0$ when the reverse inequality holds. Hence treatment should be paired with reduced contact and rapid clinical resolution. The auxiliary ϵ_F calculation also shows that any residual infectiousness in failed treatment cases increases the threshold quantity, so the assumption that F is effectively isolated is epidemiologically important.

The numerical simulations are qualitative and were not fitted to actual outbreak data. This is a major limitation of the present study. Calibration to data such as the 2003 Mexico acute hemorrhagic conjunctivitis outbreak would require time-resolved information on treatment, treatment failure, isolation, and recovery, which is not available in the compartmental form required here. Future

work should estimate these parameters using outbreak or clinical data and may also relax the isolation assumption for F, include age structure, or incorporate spatial heterogeneity.

Author contributions

Bashir Al-Hdaibat: Conceptualization, methodology, software, formal analysis, investigation, writing – original draft, supervision. **Mohammad A. Safi:** Conceptualization, methodology, software, formal analysis, investigation, writing – original draft, supervision. **Areej Almuneef:** Conceptualization, methodology, software, investigation, writing – original draft. **Zuhur Alqahtani:** Conceptualization, methodology, software, investigation, writing – original draft. **Mahmoud H. DarAssi:** Conceptualization, methodology, software, investigation, writing – original draft. **Omar Attoum:** Conceptualization, methodology, software, formal analysis, investigation, writing – original draft.

All authors have read and approved the final manuscript.

Use of Generative-AI tools declaration

The authors declare that they have not used Artificial Intelligence (AI) tools in the creation of this article.

Funding

This work was supported by Princess Nourah bint Abdulrahman University through the Researchers Supporting Project (PNURSP2026R742), Riyadh, Saudi Arabia.

Acknowledgements

The authors gratefully acknowledge Princess Nourah bint Abdulrahman University for its financial support. The authors also sincerely thank the academic editor and the anonymous reviewers for their careful reading of the manuscript, valuable comments, and constructive suggestions, which significantly improved its quality and clarity.

Conflict of interest

The authors declare that they have no competing interests.

References

1. V. Mbazumutima, P. Nshimirimana, A. Dembele, F. Ndayiragije, L. Todjihounde, Mathematical modelling of conjunctivitis viral disease: case of Burundi, *Open J. Appl. Sci.*, **15** (2025), 1366–1377. https://doi.org/10.4236/ojapps.2025.155096
2. R. ud Din, N. Ahmad, S. Ahmad, P. Pongsumpun, Modeling of eye infection transmitting by conjunctivitis adenovirus: deterministic and stochastic approach, *Eur. J. Pure Appl. Math.*, **18** (2025), 6364. https://doi.org/10.29020/nybg.ejpam.v18i4.6364

3. G. Sikazwe, Modelling acute hemorrhagic conjunctivitis in East Africa: an integrated approach to transmission dynamics and outbreak response strategies, *Preprint at SSRN*, 2025.
4. M. Zulfiqar, S. Rafique, A. Habib, A. Qader, A. Asghar, R. Riaz, Conjunctivitis infection: a brief review on its classification, etiology and therapeutic interventions, *Biol. Clin. Sci. Res. J.*, **2024** (2024). https://doi.org/10.54112/bcsrj.v2024i1.780
5. A. Mueller, Allergic conjunctivitis: an update, In: C. Traidl-Hoffmann, T. Zuberbier, T. Werfel, *Allergic diseases – From basic mechanisms to comprehensive management and prevention*, Springer, Cham, 2021, 95–99. https://doi.org/10.1007/164_2021_491
6. S. J. Ono, M. B. Abelson, Allergic conjunctivitis: update on pathophysiology and prospects for future treatment, *J. Allergy Clin. Immunol.*, **115** (2005), 118–122. https://doi.org/10.1016/j.jaci.2004.10.042
7. M. A. Pallansch, Enterovirus infections, including poliomyelitis, In: R. L. Guerrant, D. H. Walker, P. F. Weller, *Tropical infectious diseases: principles, pathogens and practice*, 3 Eds., Saunders, 2011, 398–405. https://doi.org/10.1016/B978-0-7020-3935-5.00060-4
8. S. Resnikoff, D. Pascolini, D. Etya'ale, I. Kocur, R. Pararajasegaram, G. P. Pokharel, et al., Global data on visual impairment in the year 2002, *Bull. World Health Organ.*, **82** (2004), 844–851.
9. V. H. Hu, E. M. Harding-Esch, M. J. Burton, R. L. Bailey, J. Kadimpeul, D. C. W. Mabey, Epidemiology and control of trachoma: systematic review, *Trop. Med. Int. Health*, **15** (2010), 673–691. https://doi.org/10.1111/j.1365-3156.2010.02521.x
10. J. Suksawat, S. Naowarat, Effect of rainfall on the transmission model of conjunctivitis, *Adv. Environ. Biol.*, **8** (2014), 99–104.
11. G. Chowell, E. Shim, F. Brauer, P. Diaz-Dueñas, J. M. Hyman, C. Castillo-Chavez, Modelling the transmission dynamics of acute haemorrhagic conjunctivitis: application to the 2003 outbreak in Mexico, *Stat. Med.*, **25** (2006), 1840–1857. https://doi.org/10.1002/sim.2352
12. B. Unyong, S. Naowarat, Stability analysis of conjunctivitis model with nonlinear incidence term, *Aust. J. Basic Appl. Sci.*, **8** (2014), 52–58.
13. O. M. Ogunmiloro, Stability analysis and optimal control strategies of direct and indirect transmission dynamics of conjunctivitis, *Math. Methods Appl. Sci.*, **43** (2020), 10619–10636. https://doi.org/10.1002/mma.6756
14. K. S. Nisar, A. Ahmad, M. Farman, E. Hincal, A. Zehra, Modeling and mathematical analysis of fractional order eye infection (conjunctivitis) virus model with treatment impact: prelicence and dynamical transmission, *Alex. Eng. J.*, **107** (2024), 33–46. https://doi.org/10.1016/j.aej.2024.07.020
15. S. Mangala, E. Bonyah, V. S. Sharma, Y. Yuan, A novel fractional-order stochastic epidemic model to analyze the role of media awareness in the spread of conjunctivitis, *Healthcare Anal.*, **5** (2024), 100302. https://doi.org/10.1016/j.health.2024.100302
16. F. Javed, A. Ahmad, A. H. Ali, E. Hincal, A. Amjad, Investigation of conjunctivitis adenovirus spread in human eyes by using bifurcation tool and numerical treatment approach, *Phys. Scr.*, **99** (2024), 085253. https://doi.org/10.1088/1402-4896/ad62a5

17. M. Tashfeen, H. S. Jassim, F. Dayan, M. A. Rehman, A. D. Zoltán, H. A. Neamah, An analytical approach to modeling conjunctival viral disease using fuzzy logic and time-delay dynamics, *Healthcare Anal.*, **8** (2025), 100404. https://doi.org/10.1016/j.health.2025.100404

18. W. Li, L. Yang, J. Cao, Threshold dynamics of a degenerated diffusive incubation period host-pathogen model with saturation incidence rate, *Appl. Math. Lett.*, **160** (2025), 109312. https://doi.org/10.1016/j.aml.2024.109312

19. W. Li, Y. Zhang, J. Ji, L. Huang, Dynamics of a diffusion epidemic SIRI system in heterogeneous environment, *Z. Angew. Math. Phys.*, **74** (2023), 104. https://doi.org/10.1007/s00033-023-02002-z

20. W. Li, Y. Guan, J. Cao, F. Xu, A note on global stability of a degenerate diffusion avian influenza model with seasonality and spatial heterogeneity, *Appl. Math. Lett.*, **148** (2024), 108884. https://doi.org/10.1016/j.aml.2023.108884

21. W. Li, L. Zhang, J. Cao, F. Xu, Z. Cai, Finite time attractivity and exponentially stable of a multi-stage epidemic system with discontinuous incidence, *Qual. Theory Dyn. Syst.*, **24** (2025), 199. https://doi.org/10.1007/s12346-025-01358-z

22. W. Li, Y. Zhang, Q. Ding, J. Yu, Exponential convergence of a diffusive SIRS epidemic model with standard incidence, *J. Geom. Anal.*, **36** (2026), 13. https://doi.org/10.1007/s12220-025-02251-6

23. B. Al-Hdaibat, M. Z. Meetei, I. Ahmad, N. Althobaiti, M. A. Safi, M. A. Khan, et al., The dynamics of monkeypox disease under ψ–Hilfer fractional derivative: application to real data, *Results Phys.*, **55** (2023), 107127. https://doi.org/10.1016/j.rinp.2023.107127

24. Z. Alqahtani, A. Almuneef, M. H. DarAssi, Y. AbuHour, M. Al-arydah, M. A. Safi, et al., Mathematical analysis of fractional Chlamydia pandemic model, *Sci. Rep.*, **14** (2024), 31113. https://doi.org/10.1038/s41598-024-82428-1

25. B. Al-Hdaibat, M. A. Khan, I. Ahmad, E. Alzahrani, A. Akgul, Modeling and analyzing the dynamics of brucellosis disease with vaccination in the fractional derivative under real cases, *J. Appl. Math. Comput.*, **71** (2025), 5567–5588. https://doi.org/10.1007/s12190-025-02435-x

26. M. Khader, M. H. DarAssi, Residual power series method for solving nonlinear reaction-diffusion-convection problems, *Bol. Soc. Parana. Mat.*, **39** (2021), 177–188. https://doi.org/10.5269/bspm.41741

27. B. Al-Hdaibat, M. H. DarAssi, I. Ahmad, M. A. Khan, R. Algethamie, E. Alzahrani, Numerical investigation of an SIR fractional order delay epidemic model in the framework of Mittag–Leffler kernel, *Nonlinear Dynam.*, **113** (2025), 17289–17309. https://doi.org/10.1007/s11071-025-11006-5

28. B. Al-Hdaibat, A. Alameer, Bifurcation and chaos in a nonlinear population model with delayed nonlinear interactions, *Mathematics*, **13** (2025), 2132. https://doi.org/10.3390/math13132132

29. H. Alrabaiah, M. A. Safi, M. H. DarAssi, B. Al-Hdaibat, S. Ullah, M. A. Khan, et al., Optimal control analysis of hepatitis B virus with treatment and vaccination, *Results Phys.*, **19** (2020), 103599. https://doi.org/10.1016/j.rinp.2020.103599

30. B. Al-Hdaibat, M. H. DarAssi, I. Ahmad, M. A. Khan, R. Algethamie, Investigating tuberculosis dynamics under various control strategies: a comprehensive analysis using real statistical data, *Math. Methods Appl. Sci.*, 2025. In press. https://doi.org/10.1002/mma.10779

31. Centers for Disease Control and Prevention, Clinical overview of pink eye (conjunctivitis), 2024. Available from: https://www.cdc.gov/conjunctivitis/hcp/clinical-overview/index.html.

32. G. Teschl, *Ordinary differential equations and dynamical systems*, Providence, RI: American Mathematical Society, 2024.

33. O. Diekmann, J. A. P. Heesterbeek, M. G. Roberts, The construction of next-generation matrices for compartmental epidemic models, *J. R. Soc. Interface*, **47** (2010), 873–885. https://doi.org/10.1098/rsif.2009.0386

34. P. van den Driessche, J. Watmough, Reproduction numbers and sub-threshold endemic equilibria for compartmental models of disease transmission, *Math. Biosci.*, **180** (2002), 29–48. https://doi.org/10.1016/s0025-5564(02)00108-6

35. L. J. S. Allen, *An introduction to mathematical biology*, Pearson/Prentice Hall, Upper Saddle River, NJ, 2007.

36. J. E. Mahbuba, X. S. Wang, Stability analysis of biological systems under threshold conditions, *Symmetry*, **17** (2025), 1193. https://doi.org/10.3390/sym17081193

37. J. P. LaSalle, *The stability of dynamical systems*, Society for Industrial and Applied Mathematics, Philadelphia, PA, 1976. https://doi.org/10.1137/1.9781611970432

38. C. Castillo-Chavez, B. Song, Dynamical models of tuberculosis and their applications, *Math. Biosci. Eng.*, **1** (2004), 361–404. https://doi.org/10.3934/mbe.2004.1.361

39. S. Nana-Kyere, K. K. Danquah, G. K. Hoggar, J. K. K. Asamoah, E. Acheampong, E. Okyere, Dynamical modelling and optimal control of conjunctivitis epidemic, *Eng. Rep.*, **7** (2025), e70542. https://doi.org/10.1002/eng2.70542

40. G. Chowell, C. Castillo-Chavez, P. Diaz-Duenas, Characterization of an outbreak of acute hemorrhagic conjunctivitis in Mexico, 2003, *Digital J. Ophthalm.*, 2005.

AIMS Press